Performance-Based Wind Design of Tall Buildings Considering the Nonlinearity in Building Response

Smrithi Preetha Hareendran, S.M.ASCE[1]; Alice Alipour, M.ASCE[2]; Behrouz Shafei, M.ASCE[3]; and Partha Sarkar, A.M.ASCE[4]

Abstract: Over recent years, the application of performance-based design (PBD) has continually grown in the design of tall buildings and other structures excited by large wind loads. PBD has also become a mainstream approach to assess and reduce the risks in the rehabilitation of existing structures. The significant wind-related economic losses incurred every year around the world have prompted researchers to develop methods to reframe wind engineering to embrace the concepts of PBD. The main objective of performance-based wind engineering (PBWE) is to assess the adequacy of a structure in terms of the decision variables (DVs) set forth by the stakeholders. Each DV is defined to satisfy specific performance levels such as operational, immediate occupancy, life safety, and collapse prevention. The performance levels are defined based on acceptable levels of strength and serviceability requirements of both structural and nonstructural components. They also reflect the probable levels of damage, casualties, downtime, and costs of repair. In this paper, a 44-story steel frame building under the action of wind loads was analyzed and evaluated using PBD. To understand the structural response under long-duration wind loads, the building was subjected to randomly varying wind loads for a duration of 30 min. Different time history analyses were conducted with wind speeds varying between 45 and 80 m/s (100 and 180 mph). The basic design wind speed of the building for the preliminary design based on static analysis was 58 m/s (130 mph). The building responses recorded include acceleration and displacement time histories at every floor level. These responses were used to evaluate the peak and root mean squared (RMS) variations of acceleration and interstory drift along the height of the building and also to make comparisons between different wind speeds. The member forces were recorded to identify the locations of plastic hinges and also to interpret any unusual variations in the recorded accelerations and displacements in the building. The fragility and loss ratio curves are presented, showing the response parameters in comparison with the limiting threshold specified by FEMA to categorize the structural components into different damage states (DSs) and corresponding costs of repair or replacement. **DOI: 10.1061/(ASCE)ST.1943-541X.0003312.**

Author keywords: Performance-based wind design (PBWD); Tall buildings; Nonlinear response; Performance objectives.

Introduction

Performance-based design (PBD) has become a mainstream approach to assess and reduce the risks in rehabilitation of existing structures. In addition to application in the field of seismic design, it has been used for design against other hazards such as vehicle collision (Au Yeung et al. 2019), aging, and earthquake (Cui et al. 2019). Application of PBD philosophy for design of tall buildings and other structures excited by wind loads has received much attention recently. The significant wind-related economic losses incurred every year around the world have prompted researchers to develop methods to reframe wind engineering to fully embrace the concepts of PBD. Performance-based wind engineering (PBWE) involves accounting for numerous sources of uncertainty. These include the variations in wind loads arising from the unpredictable nature of wind velocities and turbulence intensities and epistemic errors during measurement of data and modeling of structures in addition to the mechanical properties of the structure. Hence, the probabilistic PBWE framework has a higher potential to quantify structural reliability by acknowledging all of the uncertainties associated with the design problem.

One of the first instances of performance-based wind engineering mentioned is in the work by Paulotto and Ciampoli (2004) when they used it for vulnerability analysis of tall buildings. The framework was based on probabilistic calculations made in both the frequency and time domains. Performance-based earthquake engineering (PBEE) has been widely adopted in the structural engineering field because it efficiently provides cost-effective design solutions while accounting for the potential losses considering the performance objectives set by stakeholders. The technical basis for PBEE computes earthquake performance as a multilevel integral based on total probability theorem. Apart from developing the key concepts involved in PBWE, a significant amount of research has been dedicated to understanding and formulating methodologies to address the uncertainties involved in the estimation of wind loads acting on a structure. Spence et al. (2012, 2015) have worked on addressing these concerns but mostly in the elastic range or using simplistic postelastic modeling approaches. Petrini et al. (2013) provided the framework of PBWE, addressing its role in damage

[1]Ph.D. Candidate, Dept. of Civil, Construction and Environmental Engineering, Iowa State Univ., Ames, IA 50010. Email: smrithi@iastate.edu

[2]Associate Professor, Dept. of Civil, Construction and Environmental Engineering, Iowa State Univ., Ames, IA 50010 (corresponding author). ORCID: https://orcid.org/0000-0001-6893-9602. Email: alipour@iastate.edu

[3]Associate Professor, Dept. of Civil, Construction and Environmental Engineering, Iowa State Univ., Ames, IA 50010. ORCID: https://orcid.org/0000-0001-5677-6324. Email: shafei@iastate.edu

[4]Professor, Dept. of Aerospace Engineering, Iowa State Univ., Ames, IA 50010. Email: ppsarkar@iastate.edu

Note. This manuscript was submitted on November 24, 2020; approved on December 3, 2021; published online on June 27, 2022. Discussion period open until November 27, 2022; separate discussions must be submitted for individual papers. This paper is part of the ***Journal of Structural Engineering***, © ASCE, ISSN 0733-9445.

and loss analysis. Ciampoli et al. (2011, 2012) also applied PBWE formulations in the collapse assessment of a long-span suspension bridge and occupant comfort in tall buildings. Caracoglia et al. (2009), Caracoglia (2011), and Cui and Caracoglia (2017) presented calculations to obtain turbulent wind loads acting on low-rise and tall buildings. Optimization of the PBWE framework was has been conducted in different contexts by Tessari et al. (2017), Ierimonti et al. (2017), Huang et al. (2015), and Micheli et al. (2018, 2019, 2020a, b, c, 2021).

Despite the extensive work that has been conducted by these researchers in the formulation of PBWE, they mostly focus on the elastic response of the structures. This is probably because accounting for nonlinearities would complicate the analysis and introduce convergence issues. Additionally, the available international standards for design of structures under wind loads, unlike those for seismic loads, also do not allow the structure to enter the inelastic range of response, and there is a general expectation within the community for structures to remain elastic under wind events. However, recent damages under wind events have shown that not considering the inelastic structural response in the design stage will open the potential for unknown behavior after inelastic response at the least and could pose serious threats to the occupants at the most, with failure modes that have not been accounted for during the design procedure. Furthermore, the newly developed concept of smart morphing facades (Smorphacades) by the team at Iowa State University (Jafari and Alipour 2021a, b) and Abdelaziz et al. (2021) highlights the need to consider nonlinearities in the structural system should there be issues with the performance of wind vibration mitigating facades.

In addition to the general expectations of society for buildings to remain elastic under wind events as one of the reasons for the focus on the elastic design of buildings, the longer durations of wind loads acting on structures (sometimes an hour or more compared to 60 or 90 s of earthquake) pose a major hurdle to completely apply the steps of PBEE in PBWE. For example, Huang et al. (2015) considered nonlinearity but did not account for the across-wind loads that are important in tall buildings.

In 2019, ASCE published its first set of recommendations for PBWE in the form of the Pre-Standard for Performance Based Wind-Design (ASCE 2019) to act as an alternative to the prescriptive procedures given in ASCE 07-16 (ASCE 2016). The standard provides guidelines to implement PBWE in building designs to achieve an equal or superior performance objective compared to the prescriptive design methodology provided by ASCE 07-16 (ASCE 2016). The guidelines provided include recommendations on the development of wind load model, analysis requirements, and acceptance criteria for different performance objectives. The standard requires nonlinear time history analysis of buildings to satisfy the continuous occupancy performance objective and permits the use of such analyses in designing for occupant comfort and operational performance objectives as well.

With the advancements in the computational capacity available, this paper implements the proposed PBWE methodology by following the true nature of the PBD philosophy considering nonlinearity in the response of buildings and associated uncertainties in wind loading. Furthermore, the paper makes contributions to the field of PBWE by providing prediction of turbulent wind loads at each level of the building and developing the formulation to account for along-wind, across-wind, and torsional-wind loading along the height of the building. The aerodynamic load coefficients and aeroelastic load functions were obtained from wind tunnel experiments conducted on a scaled section model in the aerodynamic/atmospheric boundary layer (AABL) Wind and Gust Tunnel at the Wind Simulation and Testing (WiST) laboratory at Iowa State University (Hou and Sarkar 2018). The aerodynamic load (drag, lift, and moment) coefficients and their derivatives with respect to angle of attack were obtained for three different mean angles of attack of wind (0°, 34°, and 90°) using section model tests in a wind tunnel. The variation of these load coefficients and their derivatives along the height of the building was not considered in this study to account for the effects of Reynolds number, upstream wind turbulence, or three-dimensional flow that occurs near the top and bottom regions of the building. The aerodynamic load coefficients and their derivatives were then used to calculate buffeting load time histories for the building based on quasisteady formulation, corresponding to synthetically generated wind speed time histories based on empirical power spectral density (PSD) functions using Kaimal spectra. Aerodynamic damping for the fundamental mode of vibration was also estimated using the aerodynamic load coefficient.

Finally, the structural time history responses in the form of deflections were converted to interstory drift limits. These were then adopted to check the design of structural and nonstructural components in the building using the limit states for different structural and nonstructural components based on their damage states as given in the FEMA (2018a) database under different wind speeds. Loss analysis was also conducted for the selected fragility groups of structural and nonstructural components.

The paper provides an extensive discussion on PBEE and its extension to develop the PBWE formulations in the next section. The various components in the basic equation of PBWE are then discussed in the following section, with specifications of the parameters used in this study. The methodology of PBWE was validated using a case study of a 44-story steel frame building subjected to wind loads. The frame sections used in the building and a brief description of the static design [based on ANSI/AISC-360-16 (AISC 2016) and ASCE 07-16 (ASCE 2016)] are also given in the paper. The building modeling and analysis in OpenSEES is then presented with discussion on the models adopted to account for the nonlinearity of the structure. A validation study for the building model system is also presented using available shake-table test results. The nonlinear static pushover analysis and modal analysis conducted on the 44-story building are then presented. The paper then proceeds to show the dynamic modeling and analysis of the building under wind loads. The results obtained from the analyses are then used to develop the fragility curves, calculate the losses on various structural or nonstructural components, and measure occupant comfort.

Review of PBEE and Extensions to PBWE

The technical basis of PBEE was first documented by the Structural Engineering Association of California in 1995 as a framework to meet system performances at any specific hazard intensity. The methodology included specific performance levels such as fully operational, operational, life safety, and near collapse, whereas the hazard intervals ranged between frequent and very rare events. FEMA 273 (FEMA 1997) and FEMA 356 (FEMA 2000), developed later by the Applied Technology Council (ATC), outline the framework for first-generation PBEE. First-generation PBEE was still largely deterministic, considering specific damage limits and evaluating their performance levels. Also, the performance targets were given at component-level measurements, and the overall system performance was assumed to be consistent with the worst performance for any component in the structure. The method also did not express system performances in terms of stakeholder interests such as downtime or repair costs or casualties. Given these shortcomings, a more efficient second-generation PBEE was developed by PEER. Under the framework developed, earthquake performance was computed as a multilevel integral (PEER equation) based on the total probability theorem. It accommodates the uncertainties in

hazard intensity, structural responses, damage states, and reports in terms of variables such as downtime or monetary losses that are of direct interest to stakeholders. The PEER equation given subsequently decomposes the process into subsets that are independent of each other and are evaluated sequentially

$$\lambda(dv) = \iiint G(dv|dm)|dG(dm|\text{edp})| \cdot |dG(\text{edp}|im)| \cdot |d\lambda(im)| \tag{1}$$

where dv = decision variable that represents specific performance levels such as no collapse, occupant safety, admissible displacements, and accelerations of the building; $\lambda(\nu)$ = mean annual exceedance frequency of the decision variable, which should not exceed the tolerable annual frequency, λ_0; dm = damage measure indicating the state of damage of different structural components; edp = engineering damage parameter that relates the structural response of the structure to the damage occurrence (accelerations and displacements); im = intensity measure of the seismic event; and $G(A|B)$ = complementary cumulative distribution function (CCDF) of A conditional on B. In PBEE, the hazard curve required for the identification of im is well established. However, a similar curve is not explicitly defined in PBWE. Following the provisions of ASCE 07-16 (ASCE 2016) for the design wind loads on a structure, the closest approximation would be to consider the maximum wind speed expected to occur at any height of the structure averaged over a given time interval. The speed would also be specific to the terrain and topographic features of the site. Another factor to be considered while adjusting the PEER equation for PBWE is the wind–structure interaction given by aerodynamic loading functions. Of these interaction parameters, ip is strongly dependent on im and structural properties. Incorporating the aforementioned factors, the mathematical formulations for PBWE modified from the PEER framework equation is given in the following:

$$P_f(dv) = \iiiint G(dv|dm) \cdot |dG(dm|\text{edp})| \cdot |dG(\text{edp}|ip)| \cdot |dG(ip|im)| \cdot p(im) \cdot \text{dim} \tag{2}$$

This equation measures the performance in terms of annual exceedance probability of threshold in terms of P_f instead of considering the mean annual rate of exceedance. Probability of failure (P_f) over all wind hazards is the acceptable failure probability for a given performance level for design of the building. P_f represents the probability of the structural response exceeding the limit state of failure. In this study, P_f can be calculated from the fragility functions of the several structural components provided over the range of wind hazards presented in Fig. 15. Fig. 1 presents the flowchart required to conduct PBWE.

The main objective of PBWE is to assess the adequacy of a structure in terms of the decision variables (*DV*s) set forth by the stakeholders. Each DV is defined to satisfy specific performance levels such as operational, immediate occupancy, life safety, and collapse prevention. The performance levels are defined based on acceptable levels of strength and serviceability requirements of both structural and nonstructural components. They also reflect the probable levels of damage, casualties, downtime, and costs of repair. Uncertainty in the performance assessment is addressed by expressing the performance levels in probabilistic terms. PBWE involves definition of wind hazards, assemblage of building performance model, analysis of the building response, development of fragility functions, and calculation of performance levels.

Wind Load Model (Intensity Measure)

The wind hazard for a specific site is defined in terms of maximum wind velocity experienced at the specified height of the building over the given averaging time (i.e., gust) while accommodating the factors accounting for terrain roughness and other topographic factors. For a given bluff body immersed in wind flow, the wind velocity fluctuations are to be converted into time-varying forces to be able to conduct nonlinear time history analysis in such a way that decision variables can be generated to ease communications with stakeholders and owners. Tall buildings are subjected to nonuniform time-varying wind loads along their height, which vibrates at random frequencies. The winds fluctuate about a mean wind speed corresponding to the height at which it acts. This is shown in Fig. 2(a). Wind models based on straight-line conditions cannot predict the structural response beyond the fundamental mode of vibration. Fig. 2(b) shows the comparison of probability density functions (PDFs) of wind speeds in Miami-Dade County, Florida, derived from two different sources. The climatological records were obtained from the archives of the National Oceanic and Atmospheric Administration (NOAA). The records over a duration of 50 years were processed and their PDFs were developed. The second curve shows the wind speed distribution generated with the design wind speed at Miami-Dade County (58 m/s) as the mean wind speed. Upon comparison of the two curves, it can be seen that the site-recorded wind speed data are distributed over a very narrow range and below 18 m/s (40 mph). Hence, to cover a wider range and account for extreme wind speeds in the study, the PDF generated based on the ASCE design wind speed is taken as the reference. The wind rose diagram for wind speeds based on meteorological data is also given in Fig. 2(c), which shows the prevalent direction of wind speeds at the location. In this study, several sets of analyses are conducted to cover 90% of wind speeds in the probability density function for 3-s mean wind speeds given by ASCE for Miami-Dade County.

It is important to know the mean basic wind speed acting on a building and its variation in the time domain for the purpose of performance-based design (PBWD). This is because these wind fluctuations with respect to time contribute to the buffeting (turbulence-induced) and self-excited (motion-induced) loads on a building, thus influencing the building wind-induced vibrations significantly. In this study, the parameters required for generating the wind-load time histories for various locations of the building along its height were extracted from wind tunnel experiments. The experiments were conducted in the AABL Wind and Gust Tunnel at the WiST Lab located at Iowa State University (Hou and Sarkar 2018). For this purpose, the aerodynamic properties of the section model of the example tall building that is subject to a two-dimensional smooth flow were extracted and applied to

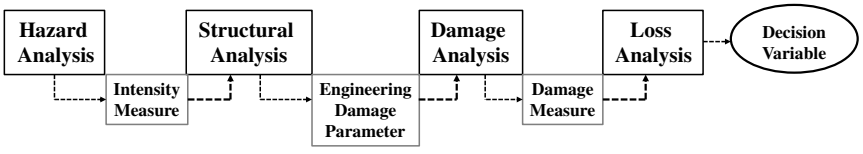

Fig. 1. Flowchart of steps involved in PBWE.

J. Struct. Eng., 2022, 148(9): 04022119

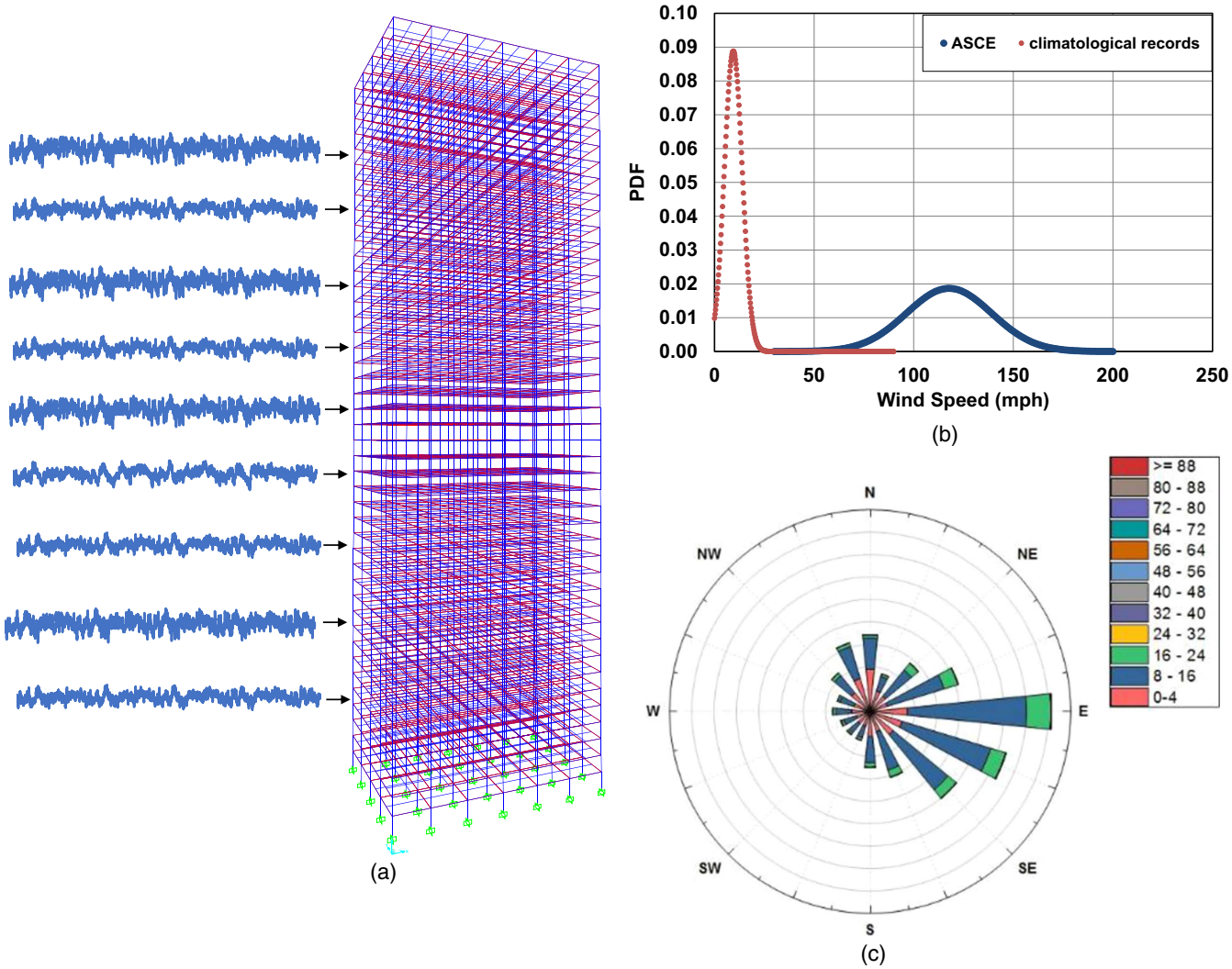

Fig. 2. (a) Schematics of fluctuating wind speed about the mean at different heights of the building; (b) PDF of wind speeds at Miami-Dade County; and (c) wind rose diagram based on NCDC data.

predict the wind loads on the tall building in time domain, where the variations of wind velocities (mean and fluctuating) in a typical atmospheric boundary-layer wind along its height were considered. A section model (1:400 scale) of the Commonwealth Advisory Aeronautical Research Council (CAARC) standard tall building (Melbourne 1980) with a rectangular cross-section was tested in the aerodynamic test section of the wind tunnel in uniform and smooth flow to obtain the static mean load coefficients. The section model dimensions are: length $L = 1.14$ m (45 in.), width $B = 0.114$ m (4.5 in.), and depth $D = 0.076$ m (3 in.) depth, with a width-to-depth ratio (B/D) of 1.5. Two 64-channel pressure transducers (Scanivalve ZOC33/64 Px) were used to measure the surface pressures on the model at 128 pressure taps, with 36 taps distributed around its cross-section at each of the three locations along the model length and 5 additional taps between these three locations along the centerline of the four faces of the cross-section. Surface pressures were integrated to obtain the mean aerodynamic loads on the model. The model was tested at various angles of attack (AOAs) ranging from 0° to 90° with increments of 5°. These tests were conducted to acquire the relationship between mean aerodynamic force coefficients (lift, drag, and moment coefficients) and AOA. The derivatives of the static load coefficients at a given AOA were then estimated using these functions.

Aeroelastic loads on flexible tall buildings are composed of buffeting and self-excited forces. The equations of motion for wind-induced response of a tall building at any height z and time t is given by Eqs. (3)–(5). Pictorial representation of the forces given subsequently are shown in Figs. 3(a and b)

$$\text{Across-wind response: } m(\ddot{h}(z,t) + 2\varsigma_h\omega_h\dot{h}(z,t) + \omega_h^2 h(z,t)) = L_B(z,t) + L_{se}(z,t) \tag{3}$$

$$\text{Along-wind response: } m(\ddot{p}(z,t) + 2\varsigma_p\omega_p\dot{p}(z,t) + \omega_p^2 p(z,t)) = D_B(z,t) + D_{se}(z,t) \tag{4}$$

$$\text{Torsional response: } I(\ddot{\alpha}(z,t) + 2\varsigma_\alpha\omega_\alpha\dot{\alpha}(z,t) + \omega_\alpha^2\alpha(z,t)) = M_B(z,t) + M_{se}(z,t) \tag{5}$$

where m = mass per unit height H of the building; I = mass moment of inertia about the centroidal axis per unit height H; $[\varsigma_h, \omega_h]$, $[\varsigma_p, \omega_p]$, and $[\varsigma_\alpha, \omega_\alpha]$ = critical damping ratio and natural frequency in the across-wind, along-wind, and torsional modes of vibration, respectively; $[\ddot{h}, \dot{h}, h]$, $[\ddot{p}, \dot{p}, p]$, and $[\ddot{\alpha}, \dot{\alpha}, \alpha]$ = acceleration, velocity, and displacement in the across-wind, along-wind, and torsional

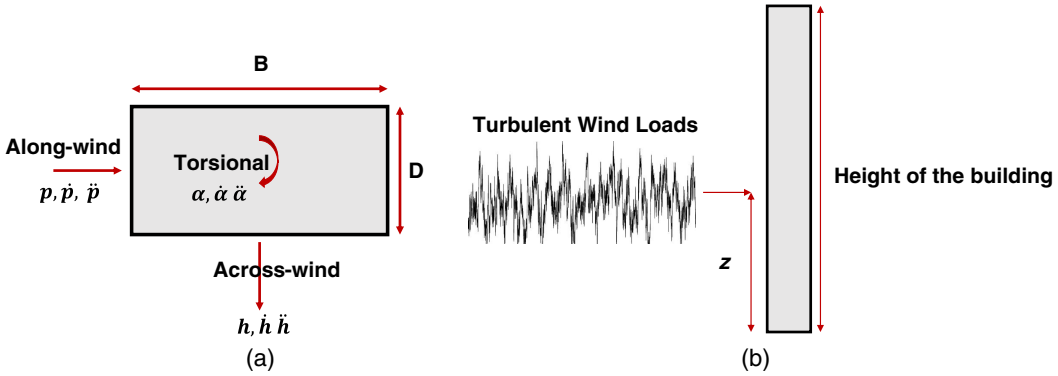

Fig. 3. (a) Forces acting on the cross-section; and (b) wind speed acting at height z of the building.

directions, respectively; $L_B(z,t)$, $D_B(z,t)$, and $M_B(z,t)$ = buffeting loads per unit height H in the across-wind, along-wind, and torsional directions; and $L_{se}(z,t)$, $D_{se}(z,t)$, and $M_{se}(z,t)$ = self-excited loads per unit height H in the across-wind, along-wind, and torsional directions acting on the structure.

Self-excited loads are due to the motion of the building under the action of buffeting wind loads. These loads act in the across, along, and torsional directions. The equations for the three self-excited load components per unit height of the building are given subsequently:

$$L_{se}(t) = \frac{1}{2}\rho U^2 B\left[\frac{KH_1^*}{U}\dot{h} + \frac{KH_2^*B}{U}\dot{\alpha} + \frac{KH_5^*}{U}\dot{p} + \frac{K^2H_4^*}{B}h + K^2H_3^*\alpha + \frac{K^2H_6^*}{B}p\right] \tag{6}$$

$$D_{se}(t) = \frac{1}{2}\rho U^2 B\left[\frac{KP_5^*}{U}\dot{h} + \frac{KP_2^*B}{U}\dot{\alpha} + \frac{KP_1^*}{U}\dot{p} + \frac{K^2P_6^*}{B}h + K^2P_3^*\alpha + \frac{K^2P_4^*}{B}p\right] \tag{7}$$

$$M_{se}(t) = \frac{1}{2}\rho U^2 B^2\left[\frac{KA_1^*}{U}\dot{h} + \frac{KA_2^*B}{U}\dot{\alpha} + \frac{KA_5^*}{U}\dot{p} + \frac{K^2A_4^*}{B}h + K^2A_3^*\alpha + \frac{K^2A_6^*}{B}p\right] \tag{8}$$

where B = width of the section model, measured in the along-wind direction; H_i^*, P_i^*, and A_i^* = known as flutter derivatives, which are functions of normalized wind speeds known as reduced velocity ($RV = U/nB, K = \omega B/U$) and the cross-sectional shape of the model, obtained from the wind tunnel tests conducted on section models; U is mean wind speed; $n = n_{h,p,\alpha}$ = natural frequency (Hz) of the model associated with the three degrees of freedom as in Eqs. (3)–(5) at zero wind speed; $\dot{h}$, $\dot{\alpha}$, and $\dot{p}$ = velocity components in the across, along, and torsional directions, and h, p, and α = displacements in the across, along, and torsional directions, respectively. The initial conditions applied for displacements and velocities were used to compute the self-excited loads for the first time step. The response of the structure has to be recorded at each time step and incorporated into the load calculations for the subsequent time steps. This could be done with the use of a feedback loop in the program. However, the effects of self-excited loads were incorporated into this study by substituting the mechanical damping C_{mech} of the structure with an effective damping C_{eff} that included the combined effects of both mechanical and aeroelastic damping in terms of flutter derivatives, as shown in Eqs. (6)–(8). Hou and Sarkar (2018, 2021) has discussed the need to address self-excited forces in tall buildings in addition to buffeting forces. This could be explored in future studies. The effects of aeroelastic stiffness on the overall stiffness of the building were neglected in this analysis. Rayleigh damping (used in the modeling of damping in OpenSees version 3.0.3) was used here to construct a damping matrix in a classical formulation. It is a viscous damping model that is a combination of damping proportional to the stiffness and inversely proportional to the mass of the structure. It estimates the modal damping ratio for the higher modes of vibration of the structure that vary with the frequency of the modes using the damping ratio of the first two modes of vibration that are either assumed or known from measurements. An eigenvalue analysis is necessary prior to determining the damping ratios corresponding to the higher modes that use the first two natural frequencies of the system for its estimation. From the modal analysis, it was observed that the first two modes of vibration are in the longitudinal and lateral directions of the building, whereas higher modes (from the fifth mode) were torsional in nature. The effective damping of the fundamental mode (along-wind) at a given wind speed (U) can be estimated using the relationship in Eq. (9*a*), where the mechanical damping ratio is assumed as 1.5%, ω is taken as the fundamental frequency, and the flutter derivative $P_1^*(K)$ that defines the aerodynamic damping is estimated from quasisteady (QS) theory [Eq. (9*b*)]. The Rayleigh damping (mechanical damping) for the higher modes was calculated based on the first two modal frequencies of vibration, whereas the aerodynamic damping for the second and higher modes, including torsional mode, was ignored here. This can be justified because the magnitudes of flutter derivatives (FDs) associated with aerodynamic damping in a specific mode become very small compared to the mechanical damping as modal frequency increases or reduced velocity decreases at the specific wind speeds considered here:

$$C_{\text{eff}} = C_{\text{mech}} + C_{\text{aero}} = C_{\text{mech}} - \left(\frac{\rho B^2\omega}{2m}\right)P_1^*(K) \tag{9a}$$

$$P_1^* = -\frac{2}{K}C_D \tag{9b}$$

where m = mass per unit height of the building; and ω = natural frequency in the fundamental mode of vibration. The drag coefficient C_D used in Eq. (9*b*) was obtained from wind tunnel tests conducted on a scaled model of a cross-section with the same aspect ratio as the plan of the building. The study assumed a constant C_D along the height of the building and hence a constant P_1^* for the building at a given reduced velocity.

Buffeting represents the turbulence-induced loads on a tall building. The wind acting on a tall building excites it under the

action of a mean wind speed $U(z)$ at elevation z from the ground and time-varying or turbulence components $u(z,t)$ and $v(z,t)$ in the along-wind and across-wind directions about the mean wind speed $U(z)$. The turbulent time histories were generated based on the algorithm proposed by Deodatis (1996). The process involved generating the $[n \times n]$ cross-spectral density matrix, where n denotes the number of variates or time histories to be generated. The elements of the matrix were derived based on power spectral density functions (PSDFs) given by Kaimal et al. (1972). The PSD function for the longitudinal turbulence component u can then be calculated using Eq. (10)

$$S_{uu}(z,\omega) = \frac{1}{2}\frac{200}{2\pi}u_*^2\frac{z}{U(z)}\frac{1}{\left[1+50\frac{\omega z}{2\pi U(z)}\right]^{5/3}} \tag{10}$$

where u_* = friction velocity; and ω = circular frequency, with an upper cutoff frequency beyond which the elements of the cross-spectral density maybe assumed as zero. The elements of an $[n \times n]$ cross-spectral density matrix are given as

$$S_{jj}(\omega) = S_j(\omega) \tag{11}$$

$$S_{jk}(\omega) = \sqrt{S_j(\omega)S_k(\omega)}\gamma_{jk}(\omega) \tag{12}$$

In Eq. (12), $\gamma_{jk}(\omega)$ is the coherence function between velocity fluctuations between the variates and is given by

$$\gamma_{jk}(\omega) = \exp\left[-\frac{\omega}{2\pi}\frac{C_z\Delta z}{\frac{1}{2}(U(z_1)+U(z_2))}\right] \tag{13}$$

$$\Delta z = z_2 - z_1 \tag{14}$$

The cross-spectral density matrix is then decomposed using Cholesky's method. The elements along the diagonal of the lower triangular matrix obtained after decomposition are real, and the off-diagonal terms are complex functions. The stochastic process given by $f_j(t)$ can then be simulated by the series given by Eq. (15) as $N \to \infty$. The simulations were performed using fast Fourier transforms (FFTs)

$$f_j(t) = 2\sum_{m=1}^{n}\sum_{l=1}^{N}|H_{jm}(\omega_{ml})|\sqrt{\Delta\omega}\cos[\omega_{ml}(t) - \theta_{jm}(\omega_{ml}) + \varphi_{ml}] \tag{15}$$

where $H_{jm}(\omega_{ml})$ = elements of the matrix obtained after the Cholesky decomposition. The obtained turbulent time histories were converted to buffeting loads. The expressions for buffeting loads based on quasisteady theory were adopted here, where for typical turbulence intensities present in the atmosphere, it may be assumed that the squares of the velocity fluctuations are negligible with respect to the square of the mean wind speed and that the load coefficients are independent of the frequency in the range considered. The equations for the buffeting loads in quasisteady theory are given by Eqs. (16)–(18)

$$D_B(t) = \frac{1}{2}\rho U(z)^2 Bh\left[C_D\left(1+2\frac{u(z,t)}{U(z)}\right) + \left(\frac{dC_D}{d\theta} - C_L\right)\frac{v(z,t)}{U(z)}\right] \tag{16}$$

$$L_B(t) = \frac{1}{2}\rho U(z)^2 Bh\left[C_L\left(1+2\frac{u(z,t)}{U(z)}\right) + \left(\frac{dC_L}{d\theta} + C_D\right)\frac{v(z,t)}{U(z)}\right] \tag{17}$$

$$M_B(t) = \frac{1}{2}\rho U(z)^2 B^2 h\left[C_M\left(1+2\frac{u(z,t)}{U(z)}\right) + \left(\frac{dC_M}{d\theta}\right)\frac{v(z,t)}{U(z)}\right] \tag{18}$$

where h = mean story height of the building at height z; C_D, C_L, and C_M = aerodynamic load coefficients for drag, lift, and torsional moments, respectively; and $dC_D/d\theta$, $dC_L/d\theta$, and $dC_M/d\theta$ = corresponding derivatives of these coefficients with respect to angle of attack (θ), all of which were obtained from the wind tunnel tests. These coefficients and their derivatives are dependent on the angle of attack θ. The aerodynamic load coefficients in Eqs. (16)–(18) were obtained from wind tunnel tests on scaled models of cross-section of the building. Hence, the aerodynamic load coefficients and their derivatives used in the wind load model are assumed to be constant over the height of the building. This limitation can be addressed by extracting the aerodynamic load coefficients from wind tunnel tests on scaled models of buildings. These coefficients and their derivatives are dependent on the angle of attack (θ) of wind with respect to the building on the horizontal plane, as given in Table 1 (normalized by dynamic pressure $\frac{1}{2}\rho U^2$ and building dimension B) obtained from the wind tunnel tests. The buffeting loads in the along-wind, across-wind, and torsional directions are considered in this study.

Vortex shedding can indeed be a major concern for very tall buildings and slender structures under the action of wind loads. Tall buildings can shed similar-sized vortices along their height when they have a uniform shape and are subjected to steady wind actions. However, across-wind response due to vortex shedding usually exceeds along-wind response only in tall buildings with a height aspect ratio greater than 3 (Liang et al. 2002). When the frequency of vortex shedding (f_s) is equal to the natural frequency (f_n) of the building, the across-wind vibrations are amplified, and the range of velocities over which they occur is called the lock-in velocity range. Vibration regimes in structures due to vortex shedding are classified as outside or inside the lock-in range. The vibrations are quite small outside the lock-in range, which covers a range of wind speeds or vortex frequencies bracketing the natural frequencies of the structure (Ehsan and Scanlan 1990). The expected vortex induced vibrations (VIVs) of a tall building can be checked with knowledge of the Strouhal number. The Strouhal number ($\mathrm{St} = f_s D/U$) for a building cross-section with B/D ratio of 1.5 at a 0° angle of attack, as used here, is given as 0.10 by Knisely (1990). Substituting the values of structural frequency, cross-sectional dimension, and Strouhal number, the lock-in velocity for the building is reported in the range of 11 m/s (24 mph) to 33.5 m/s (75 mph) corresponding to the first five modes of vibrations. Because this study focused on extreme wind effects at high wind speeds (45–80 m/s) that are much higher than those calculated for VIV and outside the lock-in range, the effects of VIV are negligible and were neglected in this study for the sake of simplification (Martin et al. 2019; Teoh et al. 2019). However, the response from VIV is amplified inside the lock-in range and should be considered for the design of tall buildings. The directionality of wind has not been explicitly

Table 1. Aerodynamic coefficients for rectangular section with $B/D = 1.5$

AOA	C_D	C_L	C_M	$\frac{dC_D}{d\theta}$	$\frac{dC_L}{d\theta}$	$\frac{dC_M}{d\theta}$
0	1.21	0	0	0.00	−3.55	−0.573
34	1.26	0.38	0.057	−3.00	−0.23	0.203
90	2.93	0	0	0.00	−2.74	−0.394

Note: AOA (angle of attack) = wind direction at 0 degree AOA is along the longer dimension B, and it is positive in the counterclockwise direction.

explored in the study because the building is designed without the knowledge of the orientation of the worst wind. However, the directionality factor of K_d given by ASCE 07-16 (ASCE 2016) was taken as 1.0 in the calculation of wind loads during the design of building. Hence, there was no reduction of wind loads based on directionality of wind, which led to a more conservative design. The design can be improved by conducting wind tunnel studies considering the directionality effects as an alternative to the design specifications given by ASCE 07-16.

The self-excited and buffeting loads described in this section incorporated wind–structure interaction through flutter derivatives and aerodynamic coefficients in the equations for drag and lift forces and torsional moments. The interaction parameters (IPs) modeled the interaction of the structure with the environment. They were highly dependent on the structural properties and wind load models used in the analysis. All values of IPs were considered deterministic and taken to be equal to the mean values.

Structural Analysis

Nonlinear response history analysis is an appropriate tool available for predicting building response at varying levels of hazard intensities. Various aspects of nonlinear analysis, such as acceptance criteria, element discretization, and assumptions on modeling of energy dissipation through viscous damping, must be tailored to the specific features of the analytical representation of the system. The necessary components of the structural model required to capture the nonlinear response and also to provide an accurate representation of the system can be chosen from building performance models. Building performance models are a collection of data presenting the building assets at risk and their exposure to wind hazards. The data contain the damage that the structural and nonstructural components (fragility groups and performance groups) can sustain and its consequences on the occupant safety in terms of life-threatening debris generation and repair costs. It also contains the location of each component within the structure and its vulnerability to wind hazards. It could also include details on the occupancy of the building (population models) and its distribution of population over the time of the day and throughout the year. The population models are generated for office spaces, education, healthcare, hospitality and multiunit residential centers, research laboratories, and retail stores.

The elements and components vulnerable to damage are assigned fragility specifications which includes the component damage states, fragility functions, and consequence functions. A fragility group is a collection of components with the same damageability and consequences of damage. This could be on account of similarity in construction and installation techniques, potential modes of damage, vulnerability to wind demands, and potential causes resulting from damage. The details on the fragility groups are available in the FEMA database called the fragility database [FEMA P-58-3 (FEMA 2018c)]. Fragility groups are further subclassified into performance groups. A performance group contains components that are subjected to the same design loads. They are classified based on the story-drift and floor accelerations and are typically categorized based on story level and direction of orientation. The interest of this study was the exceedance probability of the largest system response, also called the engineering demand parameters (EDPs) defined as Y over a threshold value. The structural responses used in the study are the interstory drifts and floor accelerations. The story-drift ratios given in the FEMA database offer much more specific limits based on the progression of damage for structural and nonstructural components. This is not available in the standard codes and specifications, where only general story-drifts are given based on a pass or fail criterion. The fragility groups selected for this paper are given in Table 2. To provide a comparison, the drift-limit criteria available in various international codes and standards are also given in Table 3. It can be seen that there are very few limits that can be obtained from the standards, and none of them provide limits based on damage progression.

The drift limits taken from the FEMA database that are more component specific were used in the fragility and loss analysis in this paper. Discussion on this is presented later in the paper. Tall buildings are also expected to ensure occupant comfort during building motion in addition to satisfying strength and serviceability requirements to preserve the integrity of the structure. Property developers and building owners continue to face a significant challenge in ensuring occupant comfort in high-rise structures with complex geometry. However, when such motion is not accounted for, the occupants of high-rise buildings can feel uncomfortable, leading to various psychological and physiological impacts on them and reduced productivity levels in work environments. High building accelerations can cause discomfort to occupants, leading to anxiety,

Table 2. Fragility groups, damage states, and drift ratio limits obtained from FEMA database

Structural or nonstructural components	Damage parameter	Damage state	Description	Median/dispersion
Welded column splices (B1031.021c)	Story drift ratio	DS1/DS2, DS3	DS1: Ductile fracture of the groove weld flange splice. Damage in field is either obscured or deemed not to warrant repair. No repair conducted.	0.02/0.4
			DS2: Ductile fracture of the groove weld flange splice.	0.02/0.4
			DS3: DS1 followed by complete failure of the web splice plate and dislocation of the two column segments on either side of the splice.	0.05/0.4
Cold formed steel walls (B1061.021a)	Story drift ratio	DS1, DS2	DS1: Pull out of sheathing fasteners from studs.	0.019/0.3
			DS2: Buckling of steel sheathing. Buckling of framing members.	0.019/0.25
Glass-type curtain walls (B2022.021)	Story drift ratio	DS1, DS2	DS1: Glass cracking.	0.0084/0.25
			DS2: Glass falls from frame.	0.0107/0.35
Gypsum wall partitions (C1011.001a)	Story drift ratio	DS1, DS2,DS3	DS1: Screw pop-out, cracking of wall board, warping or cracking of tape, slight crushing of wall panel at corners.	0.004/0.45
			DS2: Moderate cracking or crushing of gypsum wall boards (typically in corners). Moderate corner gap openings, bending of boundary studs.	0.011/0.35
			DS3: Buckling of studs and tearing of tracks. Tearing or bending of top track, tearing at corners with transverse walls, large gap openings and walls displaced.	0.019/0.25

Table 3. Limiting values of interstory drift in nonstructural components from standard building codes

Sl no.	Structural/ or nonstructural component	Drift limit	Reference standard or literature
1	Exterior walls with brittle finishes	$L/240$	International Code Council (2003)
	Exterior walls with flexible finishes	$L/120$	L: Length of wall/cladding
	Aluminum panels used in walls of sunroom additions	$L/60$	
2	Structural members supporting glass unit masonry	$L/600$	International Code Council (2003)
3	Drift of walls and frames to prevent damage to nonstructural components	$L/600$ to $L/400$ or 10 mm	ASCE 07-16 (ASCE 2016)
4	Roof drift without seismic loads	0.05 m	Foschi et al. (2002)
	Roof drift with seismic loads	$H/100$	H: height of the building
5	Walls, face loading	$h/200$	Building Research Association of
	Walls, in-plane loading	$h/500$ or 25 mm	New Zealand h: height of the wall or
	Facades or curtain walls	$h/150$	cladding
	Fixed glazing	<2× clearance or <10 mm	
	Other linings	$h/250$	
	Dynamic deflection in vibrations	<3 mm	
6	In-plane loading of walls and masonry and plaster	$h/500 < 10$ mm	Cooney and King (1988)
	Moveable partitions	$h/500 < 25$ mm	h: height of the wall or cladding unit
	In-plane loads on facades and curtain walls	$h/150$	b: clearance of window frame
	Fixed glazing	$2b < 10$ mm	
7	Interior finishes	$h/500$	National Building Code of Canada

headaches, dizziness, and nausea. The root mean squared (RMS) and peak values of accelerations are used as EDPs to address occupant comfort. RMS accelerations can be a good representation of the sensations experienced by occupants in sustained events because the duration and number of cycles of motion that occur above a threshold value may be more significant for occupants than an occasional high peak. However, occupants could also be dramatically affected by large events or peaks in response. Burton et al. (2006, 2015) and Kwok et al. (2009) presented serviceability limits on standard deviation accelerations instead of RMS accelerations because the latter does not consider the mean value. The limits were recommended based on a series of investigations conducted using motion simulators at Hong Kong University of Science and Technology (HKUST) as well as full-scale surveys. These studies aimed at addressing biodynamic reactions of the human body to building-motions, effects of such vibrations on manual tasks, cognitive performance, and occupant well-being.

Irwin (1975) was one of the first researchers stressing the need for standard design recommendations for habitability or occupant comfort in addition to strength and serviceability criteria. Based on the data from a study, he identified that accelerations controlled human perception in low-frequency vibrations (up to 1.9 Hz). Irwin (1978) expanded recommendations for limiting accelerations for occupant comfort. The recommendations were made for buildings, bridges, and other offshore structures and later served as the major foundation for development of ISO 6897 (ISO 1984) which was the first international standard developed for evaluation of occupant comfort for fixed structures such as buildings and offshore structures subjected to low-frequency vibrations. The code continues to be used today without any revisions. The standard proposes magnitudes of low-frequency horizontal motion that should produce only minimum adverse comment from people working or living in buildings. The threshold limits are recommended based on the use of the structure in case of buildings and the nature of work being carried out in the case of offshore structures. The code gives limiting horizontal motions in terms of RMS accelerations corresponding to discrete frequencies of vibrations. The limiting accelerations given by the code for buildings based on their functionality are discussed further in discussions on building responses.

The Architectural Institute of Japan (AIJ-GBV 1991) introduced the requirements to evaluate habitability in buildings subjected to wind-induced vibrations. The peak accelerations with a return period of 1 year were used in the determination of perception thresholds. Several studies were conducted in the following years by researchers to expand on these definitions (Kanda 1988, 1990; Denoon et al. 1999, 2000; Tamura 1998). Based on the evolution of such studies on habitability and occupant comfort, the AIJ-GBV was revised in 2004. AIJ-GBV (2004) covered wind-induced vibrations up to 5 Hz. This was to account for the vibrations experienced by low-rise buildings under wind loads. Fig. 4 shows the threshold curves given by the standard. Because the curves are given in terms of perception probability, it is up to the designers and building owners to choose the curve according to their requirements. The code itself does not impose regulations on the choice of curves.

Structural Model

A 44-story steel moment frame building under the wind load actions was designed for this study. The building was 160 m (528 ft) tall and had a plan aspect ratio (B/D) of 1.5:1. The steel frames were composed of beams made from wide flanged I-sections and columns of cross-rectangular sections built up with wide flanged I sections. The steel beams in the frame had a span of 8 m (26.25 ft), with

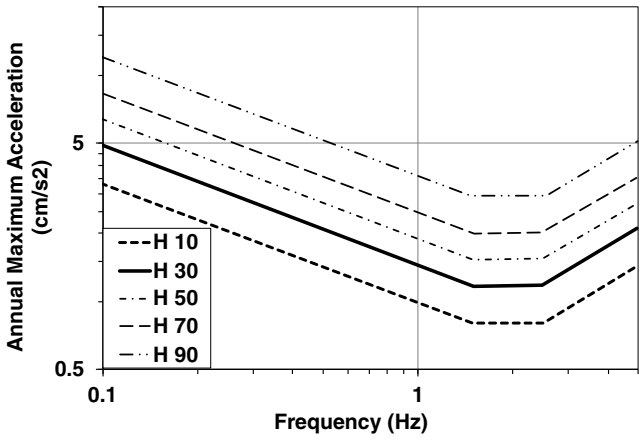

Fig. 4. Threshold accelerations given by AIJ-GBV (2004) as a function of frequency.

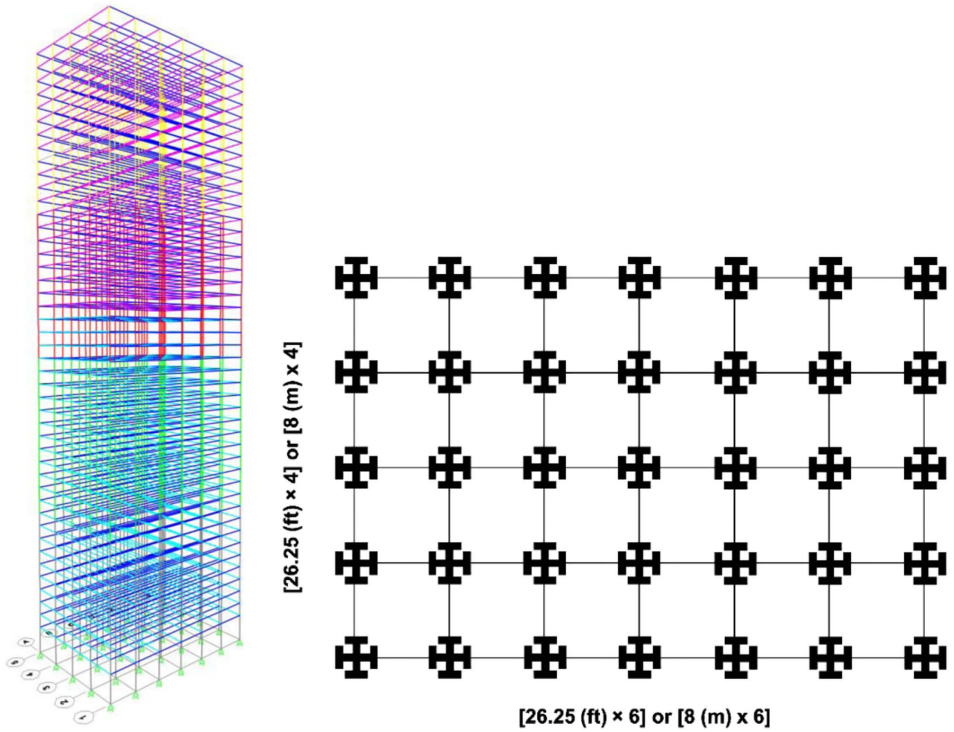

Fig. 5. Forty-four–story steel frame building: (a) 3D view of the SAP model; and (b) plan view with column sections along beam lines.

six spans along the longer direction and four in the perpendicular direction. The three-dimensional (3D) and plan views of the model are shown in Fig. 5. The building was designed under static loads based on the provisions of AISC 360 and ASCE 7 for a design wind speed of 58 m/s (130 mph) for Miami Dade county in Florida. The static analysis and design was conducted in SAP2000 (CSI 2018), and frame sections were chosen that satisfied the structural requirements.

To conduct the nonlinear time-history analysis of the whole time-history of the wind events, the structure was modeled in OpenSEES (McKenna et al. 2000). OpenSEES is a software framework for developing applications to simulate the performance of structural and geotechnical systems subjected to earthquakes. Hence, the software can perform dynamic analysis considering nonlinearities, and its use can be extended to wind analysis applications. The design of tall buildings under dynamic loads introduces a series of challenges that need to be met through consideration of scientific, engineering, and regulatory issues specific to the modeling, analysis, and acceptance criteria appropriate for these unique structural systems. ATC-72, issued by Malley and Heintz (2008), provides guidance on selection of component model types, modeling of deterioration, capture of P-Delta effects, consideration of damping, quantification of expected properties, and consideration of uncertainty. The P-delta effects on the building due to gravity and lateral loads are incorporated into the model with the use of the P-delta transformation available in the OpenSEES library. Geometric nonlinearity is attained through the transformation matrix from the natural to global coordinates. In the P-delta transformation, the matrices include the difference in transverse displacements at nodes, thus modifying the stiffness matrix.

The materials and elements available in the OpenSEES library were used in the development of the model. The nodes were assigned based on the respective story heights and frame spacing. Additional nodes at the joints were assigned to model the bilinear springs. Here the beam–column elements were modeled as displacement-based beam-column elements and zero-length elements were used to model the shear tab type beam–column connections. The gusset-to-column connections were modeled with rigid elements. Fig. 6 shows the two-dimensional (2D) representation of the line element–based model used. The springs recorded the nonlinear response of the structure. The rotational springs were modeled based on Modified Ibarra–Medina–Krawinkler deterioration model with bilinear hysteretic response. Accurate modeling of deterioration involves knowing the relevant material and geometric properties that contribute to strength and stiffness degradation in structural components. Neglecting deterioration will make it impossible to assess the performance near collapse. However, the

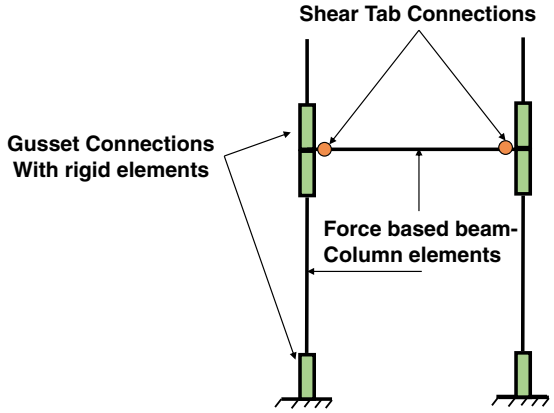

Fig. 6. 2D representation of the element-joint model used.

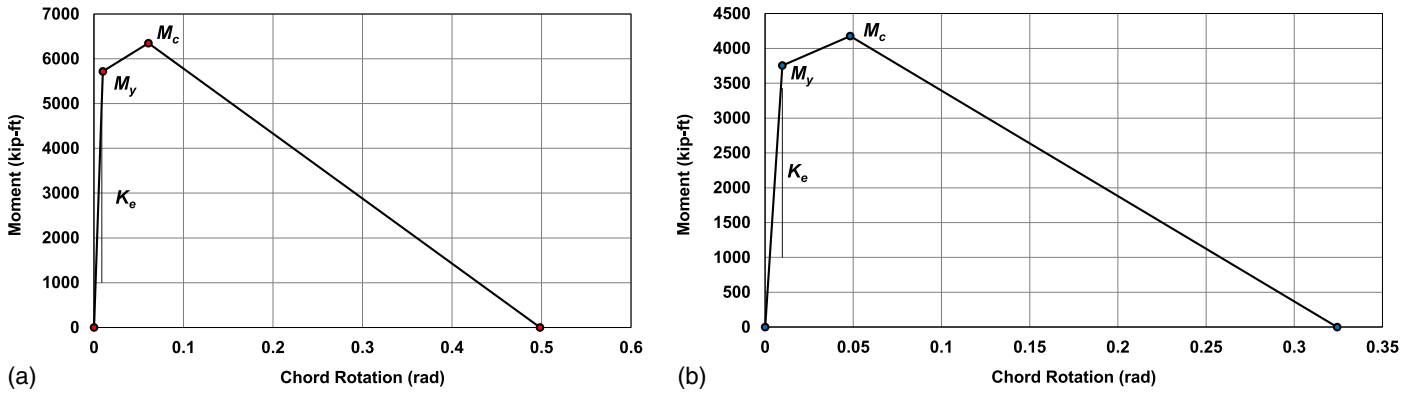

Fig. 7. Backbone curve of the beams in the transverse direction: (a) W24 × 370; and (b) W24 × 250.

accurate modeling is nearly impossible due to the inherent uncertainties associated with the material characteristics, design, and construction techniques. Moreover, an accurate deterioration model is not required because the wind actions on the building itself are highly uncertain in nature. Modeling of deterioration is equivalent to modeling the consequences of damage on the hysteretic behavior of structural components. Damage occurs due to monotonic loading and is accentuated by cyclic loading. It affects all limit states but becomes a predominant issue as a structure approaches collapse. Incorporation of deterioration becomes critical when a structure approaches collapse. The deformation associated with the capping (peak) point and the postcapping tangent stiffness are the primary parameters on which collapse capacity depends, followed closely by the rate of cyclic deterioration. Modeling of cyclic response due to deterioration is based on the concepts of a backbone curve, a set of rules that define the basic characteristics of the hysteretic behavior between the bounds defined by the backbone curve and a set of rules that define various modes of deterioration with respect to the backbone curve.

The nonlinear time history analyses in this study cover wind speeds in the range of 45 to 80 m/s (100 to 180 mph). Wind speed of 80 m/s (180 mph) in Miami, Florida, corresponds to a mean recurrence interval (MRI) of 3,000 years. The peak displacements from such a wind event are highly likely to be nonlinear. Application of cyclic wind loads at high wind speeds for long durations can lead to failure of several structural members. Studies conducted by Abdullah (2020) on reinforced concrete members under extreme wind loads demonstrated that the structural behavior of the members under wind loads are very similar to that under seismic loading. The wind loading protocol was generated to replicate the cyclic pattern equivalent to a 3-hour wind action on a building. The wind speed of 80 m/s (180 mph) corresponding to a 3,000-year MRI was chosen for the study. The results concluded that the seismically detailed beams behaved similarly under wind loads to seismic loads except for slightly less initial stiffness and more pinching in the hysteresis loops. Hence, the deterioration modeling was done using the modified Ibarra–Medina–Krawinkler model available in the OpenSEES library.

The common input parameters for the deterioration model are elastic stiffness, strain hardening ratios for positive and negative loading directions, effective yield strengths for positive and negative loading directions, rate and cyclic deterioration parameters for strength deterioration, postcapping strength deterioration, unloading and acceleration reloading stiffness deterioration, precapping and postcapping rotations for positive and negative loading directions, residual strength ratios for positive and negative loading directions, ultimate rotation capacities for positive and negative loading directions, rate of cyclic deterioration for positive and negative loading directions, and elastic stiffness amplification factor (if used for plastic hinge elements only). The backbone curves for each of the member sections were developed using an interactive web-based tool developed by Lignos and Krawinkler (2011). The tool requires the user to specify the beam full length L; the beam unbraced length L_b, which is defined as the distance from the column face to the nearest lateral brace; the expected yield stress F_y of the steel material; the capping-to-yield ratio M_c/M_y; the expected residual strength ratio K; and the ultimate rotation θ_u of the steel component. The backbone curves developed for beam sections used in the longitudinal direction of the building are shown in Fig. 7. Table 4 gives the corresponding input parameters required for the deterioration model obtained from the interactive tool.

The modeling of the joints was such that the primary nodes were fixed in their rotational degrees of freedom (DoFs) and tied to the springs that account for the rotations. The nodes at the base were modeled for fixity in the translational and rotational directions. The nodes in each floor were assigned to a diaphragm using the rigid diaphragm function. The beams and columns of the frame were composed entirely of structural steel members. The material from the OpenSees library, Steel02 (Giuffre–Menegotto–Pinto model) (Lignos and Krawinkler 2011) was used to model the members, which had a yield stress $F_y = 345$ MPa (50 ksi) and modulus of elasticity $E = 2 \times 10^5$ MPa (29,000 ksi) with isotropic hardening properties. The parameters used in the material definition to transition from elastic region to postyield behavior included a strain hardening ratio of 0.05, $R_0 = 15$, $c_{R1} = 0.925$, and $c_{R2} = 0.15$.

There are abundant data on the damping measures of tall buildings under the action of wind-induced vibrations, including several studies and standard specifications. ATC 72-1 specifies the damping range of the structure to be within 0.5% to 1% of the critical damping for steel framed buildings under serviceability checks.

Table 4. Input parameters required for the deterioration model (for beams in transverse direction)

Section	K_e kip-ft/rad (kN-m/rad)	M_y kip-ft (kN-m)	M_c kip-ft (kN-m)	M_r kip-ft (kN-m)	Θ_p (rad)	Θ_{pc} (rad)	Θ_u (rad)	Λ (rad)	K (residual strength ratio)
W24 × 370	607,187 (822,739)	5,697 (7,719)	6,323 (8,568)	2,279 (3,087)	0.051	0.437	0.06	6.314	0.4
W24 × 250	384,703.2 (521,272)	3,751 (5,082)	4,163 (5,641)	1,500 (2,033)	0.038	0.276	0.06	3.286	0.4

Table 5. Damping measures obtained from various buildings

Structure description	Damping (%)
57-story steel-frame office building	0.8
>50-story steel perimeter tube system	0.9
>50-story steel-frame tube system	1

Source: Data from Kijewski-Correa and Pirnia (2007).

Table 6. Cross-sectional details of beams and columns in the model

Cross-section	Frame element
CR50 × 3 × 40 × 3	Column (floor 1–10)
CR50 × 3 × 30 × 3	Column (floor 11–22)
CR50 × 2 × 30 × 2	Column (floor 23–33)
CR50 × 2 × 20 × 2	Column (floor 34–44)
W18 × 119	Longitudinal beam (floor 1–44)
W24 × 370	Transverse beam (floor 1–25)
W24 × 250	Transverse beam (floor 26–44)

The values are increased to 1% to 1.5% under strength limit state checks. The ISO (1997) standard specifies a damping of 1.5% for steel systems under strength checks for wind loads. The damping measured from several buildings under wind loads is given in Table 5. Based on the available literature, the structural damping for the model is set to 1.5% under strength checks.

The frame was composed of rectangular cross-sections built up from wide flanged I-sections for the columns and wide flanged I-sections for the beams. The various sections used in the model are listed in Table 6. The column and beam section dimensions were gradually reduced with increasing story levels because the loads acting on the members of higher floor levels were lower than those at the bottom levels. The sections were modeled using the fiber section function built into the OpenSEES library. This enabled modeling each section as a group of fibers with a specific uniaxial material, area, and location. The number of fibers along the width and thickness dimensions were taken as 6 and 1, respectively. The elements forming the beams were defined as displacement-based beam–column elements with concentrated plasticity through rotational springs at their ends. The mass of the structural components was defined in terms of mass density and assigned with the element definitions.

The additional loads acting on the structure included superimposed dead loads and live loads along with the wind forces. The dead and live loads were applied on the model as uniformly distributed floor loads. The calculated dead load had a magnitude of 2.4 kN/m^2 (50 lb/ft^2), and the live load had a magnitude of 3.6 kN/m^2 (75 lb/ft^2). Wind loads consisting of turbulent buffeting forces were applied to the nodes on the surface along and across the direction of wind flow.

Damage Model

The damage measure of a structure is estimated as:

$$\mathrm{DM} = \frac{\mathrm{EDP}}{C} \tag{19}$$

where C = component's capacity, as follows:

$$G(dm|\mathrm{edp}) = P(\mathrm{DM} > dm|\mathrm{edp}) = P\left(\frac{\mathrm{edp}}{C} > dm\right) \tag{20}$$

The threshold of dm is set as 1.

Validation of the Analytical Model

The validation of the suggested model was done in comparison with the collapse assessment of steel moment frames based on E-Defense full-scale shake table collapse tests. A two-by-one bay full-scale four-story steel structure was tested to collapse at the E-Defense shaking table facility in September 2007. The dimensions of the test structure were 10 × 6 m (33 × 20 ft) in the longitudinal y-direction and transverse x-direction, respectively. The story height of the structure was 3.5 m (11.5 ft), excluding the first story, which was 3.875 m (13 ft). The wide flange beams of the test structure ranged from 340 to 400 mm in depth. The steel columns were 300 × 9 hollow square sections (HSSs). The test structure was replicated in OpenSEES, and the members and joints were modeled using the elements and springs detailed in the section "Structural Model." The OpenSEES model was able to produce a fairly accurate validation of the test structure. The predominant periods of the test specimen were reported as 0.80 and 0.76 s in the x-direction and y-direction, respectively. The periods from the modal analysis were 0.74 and 0.695 s in the x-direction and y-direction, respectively. The loading protocol for dynamic shaking of the test structure consisted of progressively increased ground motion intensities of the JR Takatori motion recorded during the 1995 Kobe earthquake. All three components (two horizontal and one vertical) of this ground motion were applied simultaneously. The test specimen was subjected to a sequence of 20% (Level 1), 40% (Level 2), 60%, and 100% of the original JR Takatori record. A comparison of maximum story drift ratios along the height of the test specimen in the x-direction for 20%, 40%, and 60% testing phases is shown in Fig. 8. The figure shows the side-by-side results based on simulations from OpenSEES and experiments. From the results, it can be seen that the current modeling in OpenSEES is able to reproduce fair and accurate results of structures under nonlinear time history analysis.

Modal Analysis

A modal analysis was conducted to determine the fundamental time periods, modal frequencies, and mode shapes of the building. The modal frequencies and shapes for the first four modes are given in Fig. 9. The fundamental mode of vibration was predominantly flexure parallel to the x-axis. The higher modes were observed to be non-uniplanar (combination of flexure and torsion) in nature.

Nonlinear Static Pushover Analysis

The building was subjected to a nonlinear static pushover analysis in the shorter principal direction of the building. The analysis was carried out for gravity loads along with lateral wind loads. The building was located in Miami, Florida, and used a mean wind speed (30-min gusts of 50.5 m/s on Exposure B) of 3-sec gusts of 58 m/s (130) mph on Exposure C with a return period of 50 years for the pushover analysis. A pushover analysis using a lumped plasticity model was assumed. The analysis was conducted under displacement-controlled loading. The wind loads were calculated using the equivalent static load distribution method, detailed in ASCE 07-16 (ASCE 2016). The method used the peak base bending moment to consider the effects of inertial forces instead of peak base shear force as in seismic engineering. This allowed for accurate calculation of the gust effect factor in structures with a linear mode shape and uniform mass distribution. The equivalent static loads were calculated for the mean, background, and resonant components of the wind loads. The background and resonant wind loads were

Table 7. Limiting accelerations given by ISO 6897 (ISO 1984)

Type of structure	Frequency (Hz)	Limiting acceleration (m/s^2)
General-purpose buildings	0.067	0.081
	1.000	0.026
Special-purpose buildings	0.067	0.051
	1.000	0.014
Offshore structures	0.067	0.485
	1.000	0.156

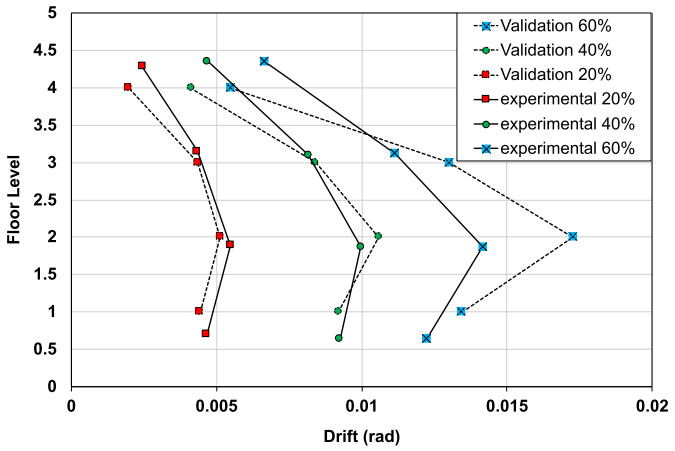

Fig. 8. Comparison of maximum story drift ratios.

expressed as a fraction of the mean wind load component dependent on the respective gust velocity factor ratios.

The wind load distribution along the height of the building is shown in Fig. 10(b). The three performance levels chosen were immediate occupancy (IO), life safety (LS), and collapse prevention (CP). The corresponding drift limits given by FEMA 273 for seismic loads were 0.7%, 2.5%, and 5% of the building height. The same was adopted in the study presented here for wind loads in the absence of any recommendation available for the same performance objectives under wind events. The goal of this study was to establish the fundamentals of performance-based engineering in the context of wind-excited tall buildings, and the assumption was that the building could experience extreme wind events well above the design wind speed of the building that could result in significant deformations. This went beyond the current prescriptive approach that assumes buildings remain elastic under design wind speeds. The assumption was validated later in the study where the drift response, though low up to the design wind speeds, increased significantly for higher wind speeds. The pushover base shear-roof drift curve is shown in Fig. 10(a). The three performance levels are shown in the figure. Locations of beam and column plastic hinges are shown in Fig. 10(c). The locations of plastic hinges are color-coded to match the performance levels and corresponding drift limits. The pushover analysis shows plastic hinge formations on columns between the 23rd and 33rd floors of the building during the life safety and collapse prevention stages. The beam hinges at the 1st, 10th, and 22nd floors were formed in the immediate occupancy drift levels, and the others were formed during the life safety and collapse prevention drift ratios.

Dynamic Time-History Analysis

To understand the structural response under long duration wind loads, the building was subjected to randomly varying wind loads for a duration of 30 min. Different time history analyses were performed with wind speeds (3-sec gust at $z = 10$ m) varying between 45 and 80 m/s (100 and 180 mph). The basic design wind speed (3-sec gust at $z = 10$ m) of the building for the preliminary design, based on static analysis, was 58 m/s (130 mph). Only the along-wind and across-wind components of the buffeting loads are considered in the dynamic analysis here. The buffeting wind loads were generated based on the formulation given in Eqs. (9) and (10), where the algorithm proposed by Deodatis (1996) was used to generate multivariate stationary stochastic wind time histories. The mean wind speed $U(z)$ was varied with the height of the building based on the power law relationship corresponding to a suburban terrain

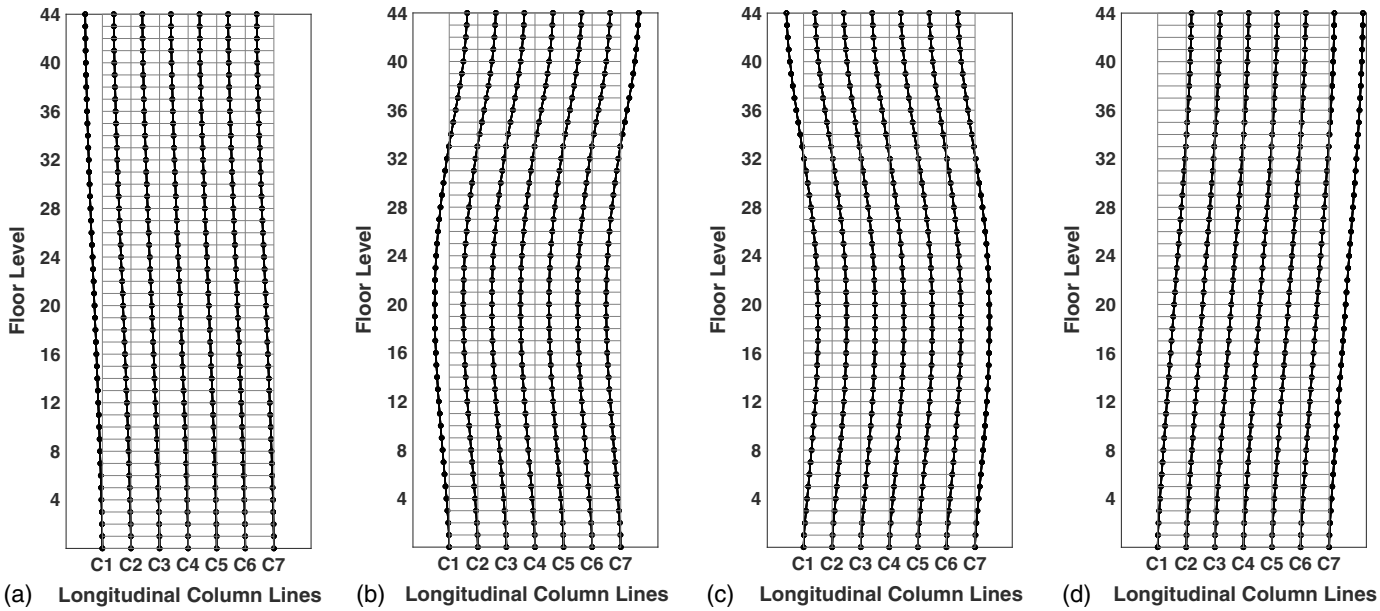

Fig. 9. Mode shapes of the building: (a) Mode 1: T = 5.42 s; (b) Mode 2: T = 2.67 s; (c) Mode 3: T = 1.87 s; and (d) Mode 4: T = 1.32 s.

J. Struct. Eng., 2022, 148(9): 04022119

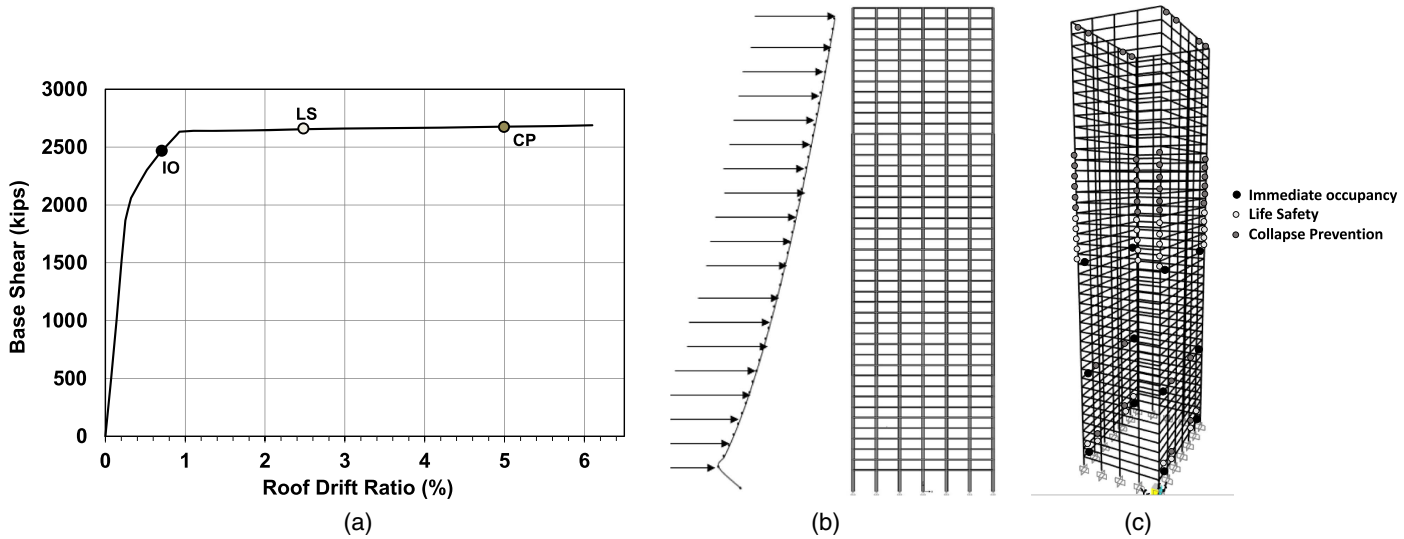

Fig. 10. (a) Base shear versus roof drift pushover curve; (b) pattern of wind loading on the building along its height; and (c) formation of plastic hinges along the height of the building.

(power law exponent of 0.23). The fluctuating velocity components $(u(z,t), v(z,t))$ of the wind time histories were generated for each floor level of the building (n variates $= 44$) considering the spatial coherence functions between the velocity fluctuations at different heights along the building. The power spectral density functions for the longitudinal u and lateral v velocity components given by Kaimal et al. (1972) were used, whereas the turbulence intensities (I_u, I_v) were varied with elevation per standard ASCE7 profiles. The sample functions were generated with the use of fast Fourier transform functions, with the lower and upper cutoff frequencies covering those from the first 10 modes of vibrations as observed from the modal analysis. A sample wind load time history (drag) at any height of the building and the variation of turbulence intensity (longitudinal) along the height of the building are shown in Figs. 11(a and b), respectively. The wind load histories that were generated by considering different tributary areas in the external and internal panels were applied at the nodes in the transverse direction at every floor level of the building.

Building Response Evaluation and Discussion

The recorded building responses include acceleration and displacement time histories at every floor level. These responses were used to evaluate the peak and RMS values of acceleration and interstory drift variations along the height of the building and also to make comparisons between different wind speeds. Due to the sudden application of wind load histories on the building, the analysis showed much higher responses (accelerations, displacements, and corresponding member forces) for a few seconds of loading at the

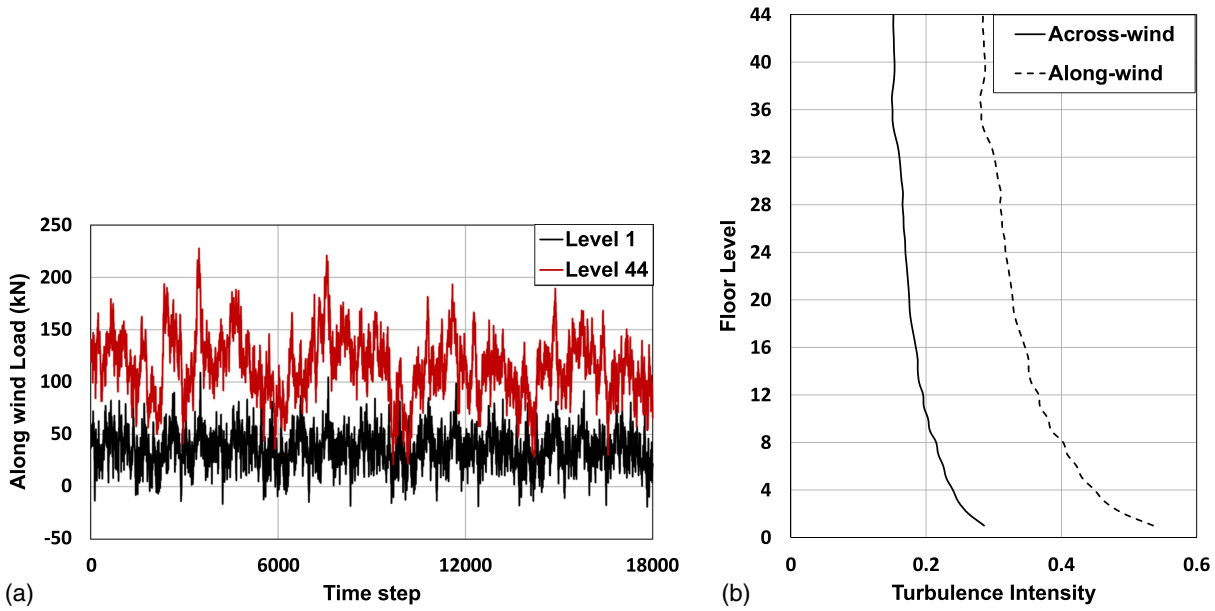

Fig. 11. (a) One realization of wind load history at 80 m/s at 1st and 44th story levels; and (b) one realization of the turbulence.

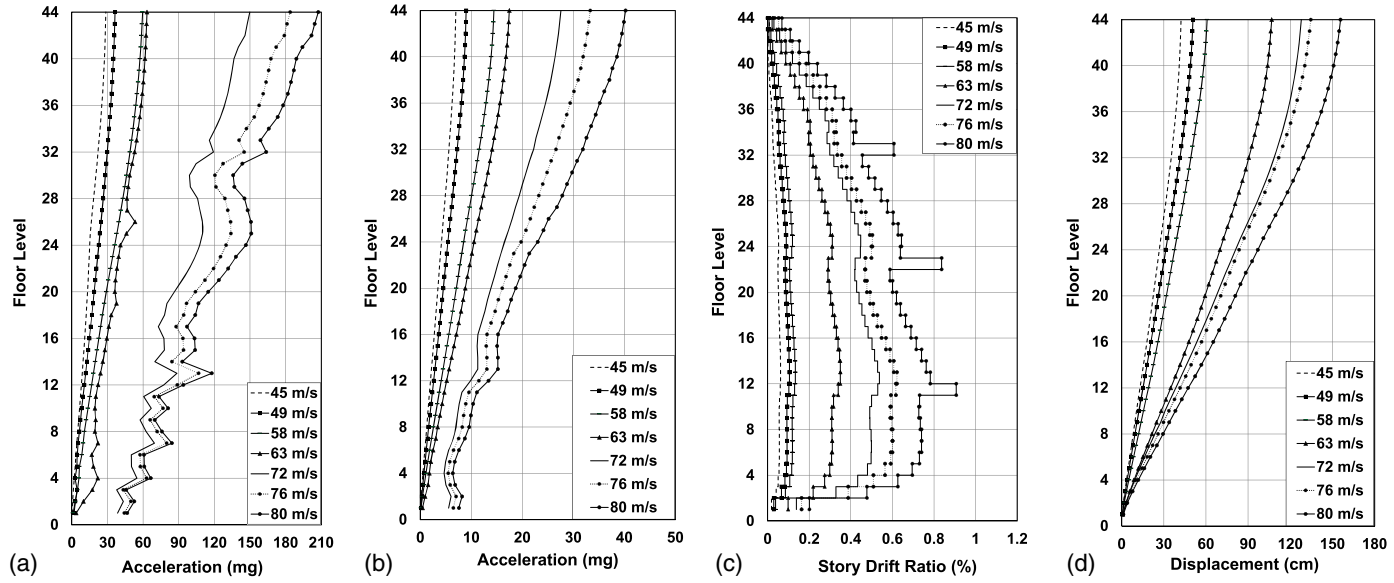

Fig. 12. (a) Peak floor acceleration; (b) RMS variation of acceleration and RMS; (c) peak interstory drift ratios; and (d) peak variations of interstory drift ratios along building height.

beginning. The initial increase was found to stabilize after the first 150 time steps, equivalent to 15 s of loading, and hence only the data beyond the 150th time step are used in the results presented here. The initial increase, though high, did not exceed the elastic range; hence, the residual effects of the higher response did not result in permanent deformations. These comparisons are presented in Figs. 12(a–d). The interstory drift ratio (IDR) is given as follows:

$$\text{IDR} = \frac{(D_i - D_{i-1})}{h} \tag{21}$$

The IDR curves (peak and RMS) showed a sudden rise in the values at three points along the height of the building. This change is associated with the reduction in column sections at these levels. The IDR values showed an increase with increasing wind speeds. Peak accelerations refer to the absolute maximum acceleration response observed for the entire duration of loading. The peak values obtained from multiple analyses for increasing wind speeds are shown in the figures given here. From the observations, it can be seen that the peak accelerations within an analysis increased with increasing height of the building. The observations were consistent for wind speeds below the design wind speed of 58 m/s (130 mph). The jaggedness in the peak accelerations at higher wind speeds can be attributed to the loss in elasticity of the members in the structure. On comparing the plots for different wind speeds, it can be seen that the peak accelerations increased with increasing wind speeds. The RMS accelerations shown in Fig. 12(b) can be compared with the limiting accelerations given in Table 7. The accelerations exceed recommended limits at design wind speed for higher floor levels. The limits are exceeded for lower floor levels (about 10th story) for very high wind speeds under long durations of loading. Hence consideration of such long durations of loading is of high importance.

The forces in every member of the structure were recorded. The member forces are required to identify the locations of plastic hinges and also to interpret any unusual variations in the recorded accelerations and displacements in the building. The capacity of the column and beam members were calculated per the provisions in AISC 360. The resistance factors given by the LRFD method specified in the code were adopted in the calculations. The capacity ratio (Force acting on the member/Design capacity of the member) was calculated for each kind of force acting on a section, and, using the interaction equations given in AISCE 360 (Chapter H), the adequacy of the member was determined. The various forces acting on the columns and beams are shown in Figs. 13(a and b), respectively.

The interaction formulae given by the code are given in Eqs. (22) and (23). P_r, V_r, T_r, and M_r represent the axial, shear, torsional, and moment forces acting on the member, and P_c, V_c, T_r, and M_c represent the axial, shear, torsional, and moment capacities of the member. The beam–column and column capacities were calculated per the provisions of AISC 360. The maximum capacity ratios for the outer windward columns in Floors 1 to 4 are shown in Fig. 14. The time-history variations of the capacity ratios are presented for two of the realizations for a wind speed of 80 m/s (180 mph), which is the highest wind speed considered in this study. The capacity ratios are shown for two different realizations of the given wind speed. The capacity ratios can be seen to reach 1.0 for columns at the second to fourth floors levels. When looking at Fig. 14 and by studying the story drift ratios of Floors 1 to 4 in Figs. 12(a and b), the drift ratios are very close to the performance level corresponding to immediate occupancy.

$$\left(\frac{P_r}{P_c} + \frac{M_r}{M_c}\right) + \left(\frac{V_r}{V_c} + \frac{T_r}{T_c}\right)^2 \leq 1.0 \tag{22}$$

$$\left(\frac{P_r}{P_{c0}}\right) + \left(\frac{M_r}{M_{cx}}\right)^2 \leq 1.0 \tag{23}$$

Fragility analysis is a standardized methodology employed in performance-based structural analysis against wind and seismic hazards. The objective of a fragility analysis is the computation of conditional probability of exceedance of damage t for engineering demand parameters such as interstory drift ratios and peak accelerations. FEMA has developed methods to correlate the response of buildings under seismic hazards to the structural and nonstructural damage and its ramifications in terms of the decision variables set by the stakeholders. The DVs may be downtime, repair costs, or casualties. The response parameters are compared with the limiting threshold specified by FEMA to categorize the structural components into different levels of damage states (DSs) upon the action of

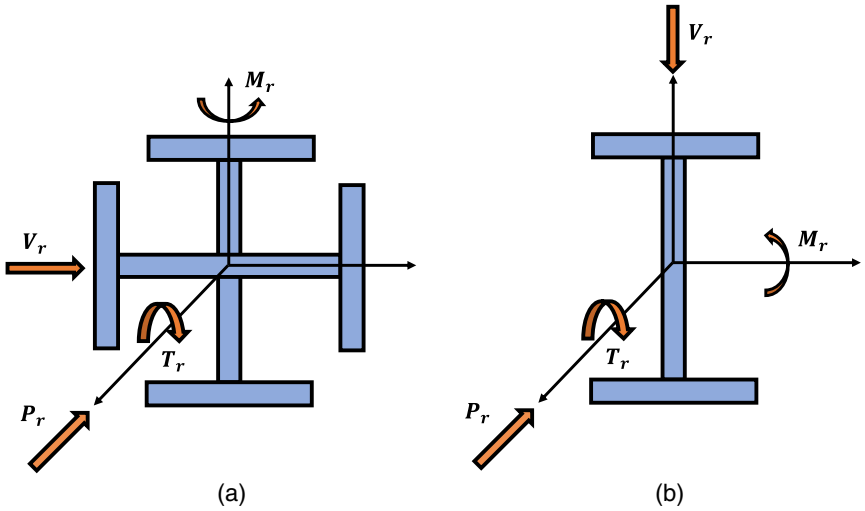

Fig. 13. (a) Forces acting on column cross-section; and (b) forces acting on beam cross-section.

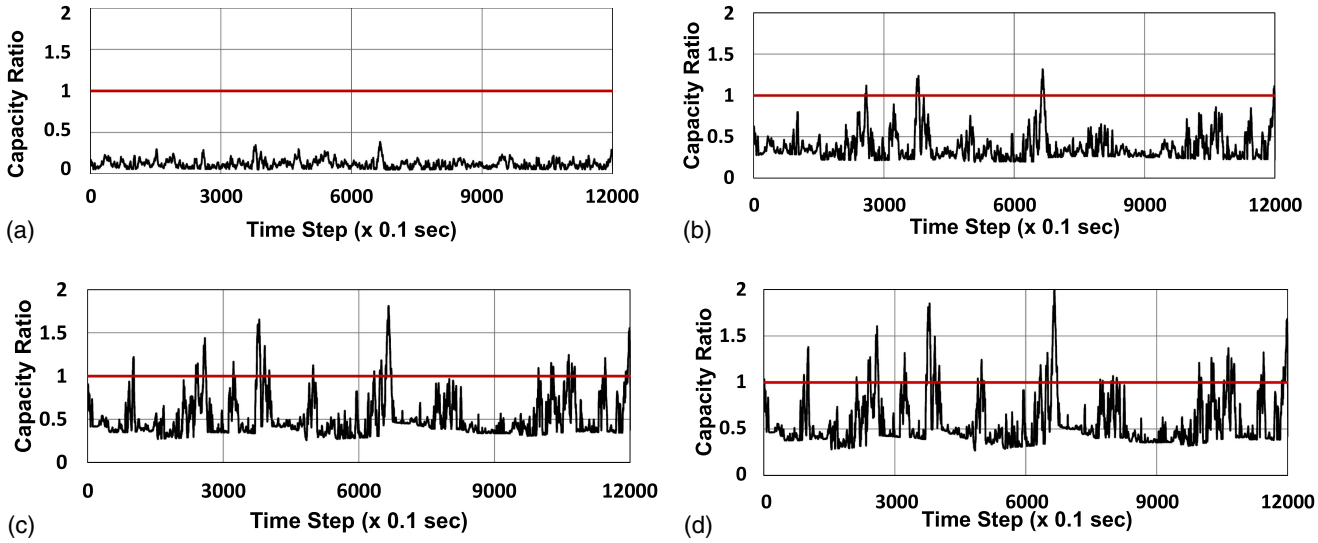

Fig. 14. Capacity ratio on column cross-section for 80 m/s for levels: (a) 1; (b) 2; (c) 3; and (d) 4. The horizontal line in all graphs shows the column capacity threshold.

wind loads. From the extensive database, five structural and nonstructural components were chosen in this study to illustrate the process. These were welded column splices, bolted shear tab gravity connections, post-Northridge welded steel moment connections, glass-type curtain walls, and gypsum partition walls. These are the fragility groups used in this study. Column 1 of Table 2 also gives annotations within parentheses to specify the fragility group label assigned by FEMA. The progress and characterization of various damage states in each of the structural or nonstructural components are given in column 4 of Table 2. For example, in the case of glass-type curtain walls, cracking of the glass would represent the first damage state (DS1), corresponding to a median interstory drift ratio of 0.0084 and dispersion of 0.25. The median and dispersion values given in the table were used to develop the lognormal probability density functions, which were then converted to cumulative density functions to obtain the fragility curves for each damage state. The same can be repeated to obtain fragility curves of different structural or nonstructural components. From the multiple variations of analyses for each set of wind speeds (between 45 and 80 m/s), the decisive percentile of interstory drift ratios can be obtained for each set of wind speeds. Twentieth percentile drift was chosen as the threshold limit IDR in this study. The probability of exceedance of the threshold IDR (P_1) can be calculated from the results of multiple sets of analysis. The probability of exceedance of drift ratios for each damage state (P_2) was then obtained by interpolation from the existing FEMA-developed fragility curves. The multiplication of P_1 by P_2 would then give the probability of exceedance of drift ratio for the damage state under the set of wind speeds. The procedure is shown in Fig. 15. The figure shows the steps to create the FEMA fragility curves as a function of edp in Step 1 and using the curves to evaluate losses due to repair or replacement of the component. The fragility curves developed using the process are shown in Figs. 16(a–e).

The cost of repair or replacement for the fragility groups is given by FEMA and can be obtained from the FEMA P-58 (FEMA 2018b) database. In this study, the loss ratio was the parameter used, which is the ratio of repair to replacement cost. Therefore, if the loss ratio is reported as 1, it means the cost of repair is either

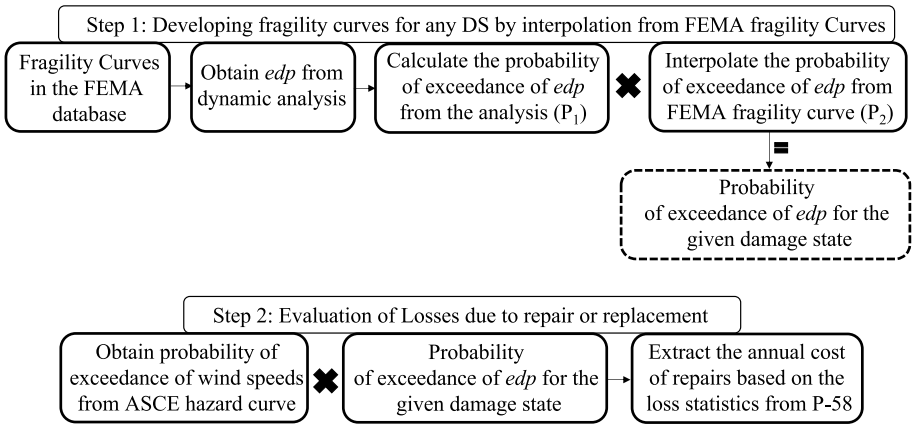

Fig. 15. Flowchart showing the development of fragility curve for any damage state of a component.

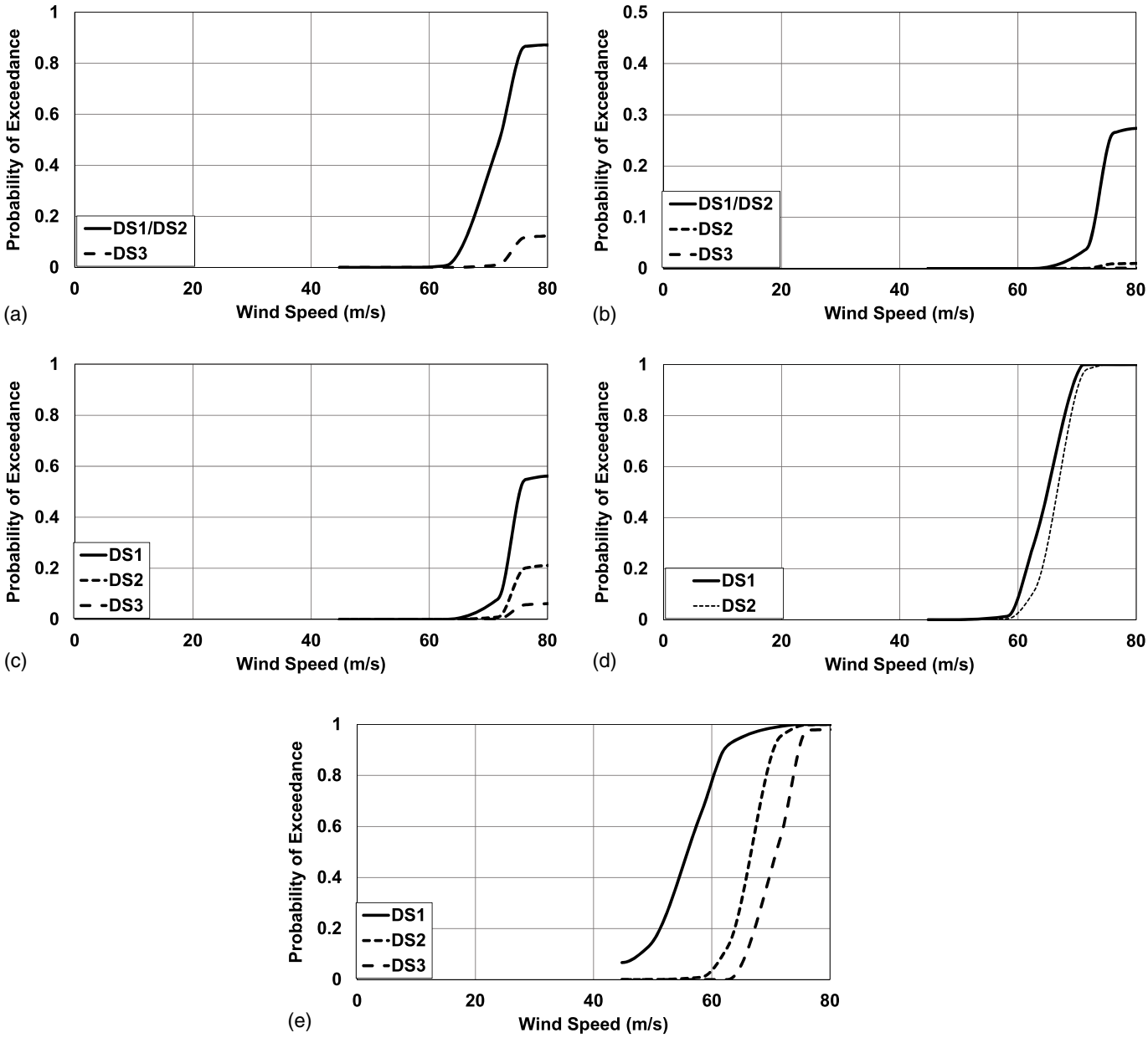

Fig. 16. Fragility curves of the various fragility groups considered in the paper: (a) welded column splices; (b) bolted shear tab gravity connections; (c) post-Northridge welded steel moment connections; (d) glass-type curtain walls; and (e) gypsum partition walls.

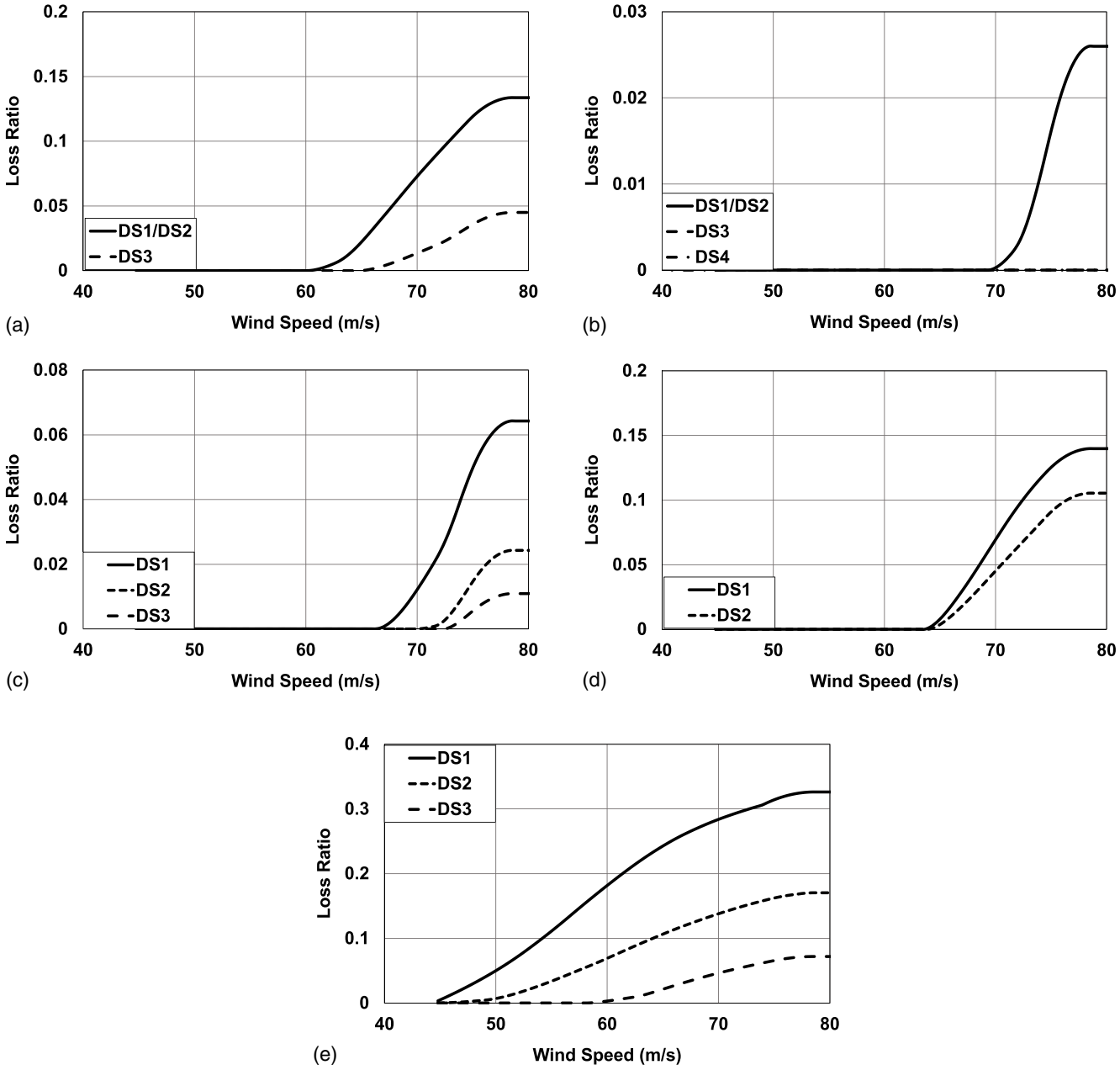

Fig. 17. Loss ratios of the various fragility groups considered in the paper: (a) welded column splices; (b) bolted shear tab gravity connections; (c) post-Northridge welded steel moment connections; (d) glass-type curtain walls; and (e) gypsum partition walls.

equal to or greater than the cost of replacement and that the component has to be replaced. The annual probability of exceedance corresponding to the highest-story drift ratio was obtained from the curves. The loss ratios for the fragility groups chosen in the study are given in Figs. 17(a–e).

The correlation between occupant comfort and floor accelerations was discussed in the previous sections. The RMS and peak accelerations presented in the previous sections were used to measure occupant comfort in the building under the given range of wind loads. When looking at the variations of peak floor accelerations, it can be seen that the values fell within the range of 25–60 mg for wind speeds up to the design wind speed. Higher wind speeds for longer durations can lead to very high peak floor accelerations where it becomes difficult to tolerate motion. However, the peak accelerations were only observed for a few seconds in the response during analysis, and hence when the criterion was RMS acceleration, the values were less than 15 mg for wind speeds up to design wind speed. This can be controlled by additional bracing at these floor levels or establishment of newer technologies such as Smrophacade.

Conclusion

This paper focused on studying the nonlinear response of tall buildings under long-duration turbulent wind loads. A 44-story steel moment-resisting frame building was designed for this purpose. The modeling criteria were validated by comparing the results with a shake-table test conducted on a steel-frame building under seismic loads. Nonlinear wind-induced pushover analysis was specifically

developed for wind loads and conducted to understand the inelastic responses of the building and identify the locations of plastic hinges under extreme wind speeds. To understand the structural response under long-duration wind loads, the building was subjected to randomly varying wind loads for a duration of 30 min. Different time history analyses were performed with wind speeds varying between 45 and 80 m/s (100 and 180 mph). The building responses recorded included acceleration and displacement time histories at every floor level. The member forces were recorded to identify the locations of plastic hinges and also to interpret any unusual variations in the recorded accelerations and displacements in the building. Multiple iterations of analyses for each set of wind speeds were used to develop fragility curves for different structural or nonstructural components in the building. The fragility curves may be used in the loss analysis of the structure. This paper provides an effective method to understand the nonlinear behavior of tall buildings under high-velocity long-duration wind loads. The fragility curves also offer an attractive methodology to optimize the design of nonstructural components of wind-sensitive high-rise buildings. From the data presented in the study on the limit states of drifts and accelerations given in the current standards, it is clear that the limit states for PBWE are not extensively presented like those given by the FEMA P-58 standards (FEMA 2018a) for PBEE. Though the PBEE limit states may be adopted for PBWE studies at present, this raises the need for availability of such a document for PBWE in addition to the available documents such as the prestandard published by ASCE. This absence of adequate data provides potential for further research.

Data Availability Statement

All data, models, or code that support the findings of this study are available from the corresponding author upon reasonable request.

Acknowledgments

This paper is based upon work supported by the National Science Foundation under Grants Nos. 1826356 and 1827774. Their support is gratefully acknowledged. Any opinions, findings, and conclusions or recommendations expressed in this material are those of the authors and do not necessarily reflect the views of the sponsor.

References

Abdelaziz, K. M., A. Alipour, and J. D. Hobeck. 2021. "A smart façade system controller for optimized wind-induced vibration mitigation in tall buildings." *J. Wind Eng. Ind. Aerodyn.* 212 (May): 104601. https://doi.org/10.1016/j.jweia.2021.104601.

Abdullah, S. 2020. "Performance of reinforced concrete coupling beams subjected to simulated wind loading." *ACI Struct. J.* 117 (3): 1.

AIJ (Architectural Institute of Japan). 2004. *Guidelines for the evaluation of habitability to building vibration*. Tokyo: AIJ.

AISC. 2016. *Specification for structural steel buildings*. ANSI/AISC-360-16. Chicago: AISC.

ASCE. 2016. *Minimum design loads on buildings and other structures*. ASCE 07-16. Reston, VA: ASCE.

ASCE. 2019. *Prestandard for performance based wind design*. Reston, VA: ASCE.

Auyeung, A., A. Alipour, and D. Saini. 2019. "Performance-based design of bridge piers under vehicle collision." *Eng. Struct.* 191 (Jul): 752–765. https://doi.org/10.1016/j.engstruct.2019.03.005.

Burton, M. D., K. C. S. Kwok, and A. Abdelrazaq. 2015. "Wind-induced motion of tall buildings: Designing for occupant comfort." *Int. J. High Rise Build.* 4 (1): 1–8. https://doi.org/10.21022/IJHRB.2015.4.1.001.

Burton, M. D., K. C. S. Kwok, P. A. Hitchcock, and R. O. Denoon. 2006. "Frequency dependence of human response to wind-induced building motion." *J. Struct. Eng.* 132 (2): 296–303. https://doi.org/10.1061/(ASCE)0733-9445(2006)132:2(296).

Caracoglia, L. 2011. "Simulation of linear and non-linear propagation effects of a random turbulence field on bridge flutter instability." *J. Wind Eng. Ind. Aerodyn.* 99 (3): 945–954. https://doi.org/10.1016/j.jweia.2011.06.001.

Caracoglia, L., and N. P. Jones. 2009. "Analysis of full-scale wind and pressure measurements on a low-rise building." *J. Wind Eng. Ind. Aerodyn.* 97 (5–6): 5–6. https://doi.org/10.1016/j.jweia.2009.06.001.

Ciampoli, M., and F. Petrini. 2012. "Performance-based Aeolian risk assessment and reduction for tall buildings." *Prob. Eng. Mech.* 28 (Apr): 75–84. https://doi.org/10.1016/j.probengmech.2011.08.013.

Ciampoli, M., F. Petrini, and G. Augusti. 2011. "Performance-based wind engineering: Towards a general procedure." *Struct. Saf.* 33 (6): 367–378. https://doi.org/10.1016/j.strusafe.2011.07.001.

Cooney, R. C., and A. B. King. 1988. *Serviceability criteria for buildings*. Porirua, New Zealand: BRANZ.

CSI (Computers and Structures Inc.). 2018. *SAP2000 integrated software for structural analysis and design*. Berkeley, CA: CSI.

Cui, W., and L. Caracoglia. 2017. "Examination of experimental variability in HFFB testing of a tall building under multi-directional winds." *J. Wind Eng. Ind. Aerodyn.* 171 (Sep): 34–49. https://doi.org/10.1016/j.jweia.2017.09.001.

Cui, Z., A. Alipour, and B. Shafei. 2019. "Structural performance of deteriorating reinforced concrete columns under multiple earthquake events." *Eng. Struct.* 191 (Jul): 460–468. https://doi.org/10.1016/j.engstruct.2019.04.073.

Denoon, R. O., W. Letchford, K. C. S. Kwok, and D. L. Morrison. 1999. "Field measurements of human reaction to wind-induced building motion." In *Proc., Wind Engineering into the 21st Century*. Rotterdam, Netherlands: Elsevier.

Denoon, R. O., R. D. Roberts, C. W. Letchford, and K. C. S. Kwok. 2000. *Field experiments to investigate occupant perception and tolerance of wind-induced building motion*. Camperdown, Australia: Univ. of Sydney.

Deodatis, G. 1996. "Simulation of ergodic multivariate stochastic processes." *J. Eng. Mech.* 122 (8): 778–787. https://doi.org/10.1061/(ASCE)0733-9399(1996)122:8(778).

Ehsan, F., and R. H. Scanlan. 1990. "Vortex-induced vibrations of flexible bridges." *J. Eng. Mech.* 116 (6): 1392–1411. https://doi.org/10.1061/(ASCE)0733-9399(1990)116:6(1392).

FEMA. 1997. *NEHRP guidelines for the seismic rehabilitation of buildings*. FEMA 273. Washington, DC: FEMA.

FEMA. 2000. *Prestandard and commentary for the seismic rehabilitation of buildings*. FEMA 356. Washington, DC: FEMA.

FEMA. 2018a. *Seismic performance assessment of buildings, volume 1—Methodology*. FEMA P-58. Washington, DC: FEMA.

FEMA. 2018b. *Seismic performance assessment of buildings, volume 2—Implementation guide*. FEMA P-58. Washington, DC: FEMA.

FEMA. 2018c. *Seismic performance assessment of buildings, volume 3—Supporting electronic materials and background documentation*. FEMA P-58. Washington, DC: FEMA.

Foschi, R. O., H. Li, and J. Zhang. 2002. "Reliability and performance-based design: A computational approach and applications." *Struct. Saf.* 24 (2): 205–218. https://doi.org/10.1016/S0167-4730(02)00025-5.

Hou, F., and P. Sarkar. 2021. "Time-domain model for prediction of generalized 3DOF buffeting response of tall buildings using 2D aerodynamic sectional properties." *Eng. Struct.* 232 (Apr): 111847. https://doi.org/10.1016/j.engstruct.2020.111847.

Hou, F., and P. P. Sarkar. 2018. "A time-domain method for predicting wind-induced buffeting response of tall buildings." *J. Wind Eng. Ind. Aerodyn.* 182 (Nov): 61–71. https://doi.org/10.1016/j.jweia.2018.09.013.

Huang, M. F., Q. Li, C. M. Chan, W. J. Lou, K. C. S. Kwok, and G. Li. 2015. "Performance-based design optimization of tall concrete framed structures subject to wind excitations." *J. Wind Eng. Ind. Aerodyn.* 139 (Apr): 70–81. https://doi.org/10.1016/j.jweia.2015.01.005.

Ierimonti, L., L. Caracoglia, I. Venanzi, and A. Luigi. 2017. "Investigation on life-cycle damage cost of wind-excited tall buildings considering

directionality effects." *J. Wind Eng. Ind. Aerodyn.* 171 (Dec): 207–218. https://doi.org/10.1016/j.jweia.2017.09.020.
International Code Council. 2003. *International building code*. Falls Church, VA: International Code Council.
Irwin, A. W. 1975. "Human reactions to oscillations of buildings-acceptable limits." *Build Int.* 8 (2): 89–102.
Irwin, A. W. 1978. "Human response to dynamic motion of structures." *Struct. Eng.* 56 (9): 237–244.
ISO. 1984. *Guidelines for the evaluation of the response of occupants of fixed structures, especially buildings and off-shore structures, to low-frequency horizontal motion (0.063-1 Hz)*. ISO 6897. Geneva: ISO.
ISO. 1997. *Steel structures-Part 1: Materials and design*. ISO 10721-1. Geneva: ISO.
Jafari, M., and A. Alipour. 2021a. "Methodologies to mitigate wind-induced vibration of tall buildings: A state-of-the-art review." *J. Build. Eng.* 33 (Jul): 101582. https://doi.org/10.1016/j.jobe.2020.101582.
Jafari, M., and A. Alipour. 2021b. "Review of approaches, opportunities, and future directions for improving aerodynamics of tall buildings with smart facades." *J. Sustainable Cities Soc.* 72 (Sep): 102979. https://doi.org/10.1016/j.scs.2021.102979.
Kaimal, J. C., J. C. Wyngaard, Y. Izumi, and O. R. Coté. 1972. "Spectral characteristics of surface-layer turbulence." *Q. J. R. Meteorol. Soc.* 98 (417): 563–589. https://doi.org/10.1002/qj.49709841707.
Kanda, J. 1988. "Probabilistic criteria for human perception of low-frequency horizontal motions." In *Proc., Symp. /Workshop on Serviceability of Buildings (Movements, Deformations, Vibrations)*. Reston, VA: ASCE.
Kanda, J. 1990. "Probabilistic perception limits of low-frequency horizontal motions." In *Proc., Conf. on Serviceability of Steel and Composite Structures*. Daejeon, South Korea: Korea Institute of Science and Technology Information.
Kijewski-Correa, T., and J. D. Pirnia. 2007. "Dynamic behavior of tall buildings under wind: insights from full-scale monitoring." *Struct. Des. Tall Special Build.* 16 (1): 471–486. https://doi.org/10.1002/tal.415.
Knisely, C. W. 1990. "Strouhal numbers of rectangular cylinders at incidence: A review and new data." *J. Fluids Struct.* 4 (4): 371–393. https://doi.org/10.1016/0889-9746(90)90137-T.
Kwok, K. C. S., P. A. Hitchcock, and M. D. Burton. 2009. "Perception of vibration and occupant comfort in wind-excited tall buildings." *J. Wind Eng. Ind. Aerodyn.* 97 (2): 368–380. https://doi.org/10.1016/j.jweia.2009.05.006.
Liang, S., S. Liu, L. Zhang, and M. Gu. 2002. "Mathematical model of acrosswind dynamic loads on rectangular tall buildings." *J. Wind Eng. Ind. Aerodyn.* 90 (12–15): 1757–1770. https://doi.org/10.1016/S0167-6105(02)00285-4.
Lignos, D. G., and H. Krawinkler. 2011. "Deterioration modeling of steel components in support of collapse prediction of steel moment frames under earthquake loading." *J. Struct. Eng.* 137 (11): 1291–1302. https://doi.org/10.1061/(ASCE)ST.1943-541X.0000376.
Malley, J., and J. Heintz. 2008. *ATC-72 of the PEER tall buildings initiative: Interim guidelines on modeling and acceptance criteria for seismic design and analysis of tall buildings*. Redwood City, CA: Applied Technology Council.
Martin, J., A. Alipour, and P. Sarkar. 2019. "Fragility surfaces for multi-hazard analysis of suspension bridges under earthquakes and microbursts." *J. Struct. Eng.* 197 (Oct): 109169. https://doi.org/10.1016/j.engstruct.2019.05.011.
McKenna, F., G. L. Fenves, and M. H. Scott. 2000. *Open system for earthquake engineering simulation*. Berkeley, CA: Univ. of California.
Melbourne, W. H. 1980. "Comparison of measurements on the CAARC standard tall building model in simulated model wind flows." *J. Wind Eng. Indus. Aerodyn.* 6 (1–2): 73–88. https://doi.org/10.1016/0167-6105(80)90023-9.
Micheli, L., A. Alipour, and S. Laflamme. 2018. "Performance-based design for wind-excited tall buildings equipped with high performance control systems." In *Proc., Structures Congress 2018: Buildings and disaster management—Selected Papers from the Structures Congress*. Reston, VA: ASCE.
Micheli, L., A. Alipour, and S. Laflamme. 2019. "Data-driven risk-based assessment of wind-excited tall buildings." In *Proc., Structures Congress 2019: Blast, Impact Loading, and Research and Education—Selected Papers from the Structures Congress*. Reston, VA: ASCE.
Micheli, L., A. Alipour, and S. Laflamme. 2020a. "Multiple-surrogate models for probabilistic performance assessment of wind-excited tall buildings under uncertainties." *J. Risk Uncertain. Eng. Syst. Part A Civ. Eng.* 6 (4): 04020042. https://doi.org/10.1061/AJRUA6.0001091.
Micheli, L., A. Alipour, and S. Laflamme. 2021. "Life-cycle cost optimization of wind-excited tall buildings using surrogate models." *Struct. Des. Tall Special Build.* 30 (6): e1840. https://doi.org/10.1002/tal.1840.
Micheli, L., L. Cao, S. Laflamme, and A. Alipour. 2020b. "Life-cycle cost evaluation strategy for high-performance control sysztems under uncertainties." *J. Eng. Mech.* 146 (2): 04019134. https://doi.org/10.1061/(ASCE)EM.1943-7889.0001711.
Micheli, L., J. Hong, S. Laflamme, and A. Alipour. 2020c. "Surrogate models for high performance control systems in wind-excited tall buildings." *Appl. Soft Comput. J.* 90 (May): 106133. https://doi.org/10.1016/j.asoc.2020.106133.
Paulotto, C., M. Ciampoli, and G. Augusti. 2004. "Some proposals for a first step towards a performance based wind engineering." In *Proc., IFED-Int. Forum Engineering Decision Making*. Enryakuji, Japan: International Forum in Engineering Decision Making.
Petrini, F., K. Gkoumas, and F. Bontempi. 2013. "Damage and loss evaluation in the performance-based wind engineering." In *Proc., Safety Reliability ICOSSAR 2013, Safety, Reliability Risk Life-Cycle Perform. Structure Infrastructures*. New York: Taylor & Francis.
Spence, S. M. J., E. Bernardini, and A. Kareem. 2015. "A first step towards a general methodology for the performance-based design of wind-excited structures." *Struct. Congress* 2015 (Apr): 1482–1493. https://doi.org/10.1061/9780784479117.127.
Spence S. M. J., and M. Gioffrè. 2012. "Large scale reliability-based design optimization of wind excited tall buildings." *Probabilistic Eng. Mech.* 28 (Apr): 206–215. https://doi.org/10.1016/j.probengmech.2011.08.001.
Tamura, Y. 1998. "Application of damping devices to suppress wind-induced responses of buildings." *J. Wind Eng and Ind. Aerodyn.* 74 (Apr): 49–72. https://doi.org/10.1016/S0167-6105(98)00006-3.
Teoh, Y. E., A. Alipour, and A. Cancelli. 2019. "Probabilistic performance assessment of power distribution infrastructure under wind events." *Eng. Struct.* 197 (Oct): 109199. https://doi.org/10.1016/j.engstruct.2019.05.041.
Tessari, R. K., H. M. Kroetz, and A. T. Beck. 2017. "Performance-based design of steel towers subject to wind action." *Eng. Struct.* 143 (Jul): 549–557. https://doi.org/10.1016/j.engstruct.2017.03.053.